

MSCoTDet: Language-driven Multi-modal Fusion for Improved Multispectral Pedestrian Detection

Taeheon Kim*, Sangyun Chung*, Damin Yeom, Youngjoon Yu, Hak Gu Kim and Yong Man Ro, *Senior Member, IEEE*.

Abstract—Multispectral pedestrian detection is attractive for around-the-clock applications due to the complementary information between RGB and thermal modalities. However, current models often fail to detect pedestrians in certain cases (e.g., thermal-obscured pedestrians), particularly due to the modality bias learned from statistically biased datasets. In this paper, we investigate how to mitigate modality bias in multispectral pedestrian detection using a Large Language Model (LLM). Accordingly, we design a Multispectral Chain-of-Thought (MSCoT) prompting strategy, which prompts the LLM to perform multispectral pedestrian detection. Moreover, we propose a novel Multispectral Chain-of-Thought Detection (MSCoTDet) framework that integrates MSCoT prompting into multispectral pedestrian detection. To this end, we design a Language-driven Multi-modal Fusion (LMF) strategy that enables fusing the outputs of MSCoT prompting with the detection results of vision-based multispectral pedestrian detection models. Extensive experiments validate that MSCoTDet effectively mitigates modality biases and improves multispectral pedestrian detection.

Index Terms—Multispectral Chain-of-Thought Detection, Language-driven Multi-modal Fusion, Multispectral Pedestrian Detection, Large Language Models.

I. INTRODUCTION

Multispectral pedestrian detection is the task of detecting pedestrians based on different visual modalities (i.e., RGB and thermal) [1]–[11]. Due to their complementary information, combining these modalities improves pedestrian detection all day/night [12]–[15]. With advances in this field, the primary interest in multispectral pedestrian detection has been focused on effectively fusing the complementary information between the two modalities. Previous works investigated various fusion methods in different stages of the network, which are often categorized as early-fusion [16], mid-fusion [12], [17], [18], and late-fusion [16], [19]. These methods demonstrated superior detection performance compared to standard pedestrian detection [20]–[30], especially in practical datasets [13], [31], [32] that contain all day/night scenarios.

Despite the progress in this task, there are still remaining

problems that need to be solved. From a recent work [17], multispectral pedestrian detection models are known to rely on spurious modality bias toward the thermal modality, due to learning the statistical bias in datasets. In multispectral pedestrian datasets, the pedestrian always statistically co-occur with its thermal signatures [17] because the thermal modality is generally robust both day/night (Fig. 1 (a)). Models trained on these datasets learn the statistical co-occurrences of thermal signatures associated with pedestrians. As a result, models often fail on test data in which such co-occurrences do not hold, e.g., pedestrians with obscured thermal signatures (or, *thermal-obscured* pedestrians). In the real world, thermal-obscured pedestrians are captured when intermediate obstacles, such as heat-insulating cloth or glass windows, block thermal radiation from reaching the thermal camera. Fig. 1 (b) demonstrates a multispectral pedestrian detector predicts the thermal-obscured pedestrian based on its absence of thermal signature, leading to failed detections. Such a phenomenon implies that modality biases limit the generalization of multispectral pedestrian detection models.

However, developing a model that performs unbiased inference is challenging from biased training. This challenge arises due to a lack of explicit visual priors in training data. While increasing supervision of these priors through extra annotations or data augmentation could be one solution, it is difficult to achieve. It is because detection failures due to modality biases are not just limited to specific cases, such as thermal-obscured pedestrians, but are common in real-world data. For example, models often mistakenly detect trees or fireplugs as pedestrians due to their similar thermal signatures. It is difficult to find all detection failure cases caused by modality biases and augment the training priors accordingly [17], [33]. And the cost of multispectral data collection and manual annotation is prohibitive [19].

Our work is motivated by the observation that prompting large language models (LLMs) [34]–[36] can produce accurate detection results on challenging data (e.g., thermal-obscured pedestrians), especially in cases where conventional detection models fail due to modality biases. As shown in Fig.1 (c), we prompt an LLM with text descriptions of both RGB and thermal images, asking, “Based on these descriptions, what is in these images?”. From these descriptions, the LLM successfully detects the thermal-obscured pedestrian based on the rationale that heat-insulating clothing makes the pedestrian invisible in thermal images. In contrast, conventional vision-based detectors often fail to detect thermal-obscured pedestrians (Fig.1 (b)). These observations motivate us to adapt

*: Both authors contributed equally to this manuscript.

This work was conducted by Center for Applied Research in Artificial Intelligence (CARAI) grant funded by DAPA and ADD (UD230017TD) (Corresponding author: Yong Man Ro).

T. Kim, S. Chung, D. Yeom, Y. Yu, and Y. M. Ro are with Integrated Vision and Language Lab., School of Electrical Engineering, Korea Advanced Institute of Science and Technology (KAIST), 291 Daehak-ro, Yuseong-gu, Daejeon, 34141, Republic of Korea (e-mail: eetaekim@kaist.ac.kr; jellarum@kaist.ac.kr; damin321@kaist.ac.kr; greatday@kaist.ac.kr; ymro@kaist.ac.kr).

H.G. Kim is with Department of Image Science and Arts, GSAIM, Chung-Ang University, Seoul, 06974, Republic of Korea (e-mail: hakgukim@cau.ac.kr).

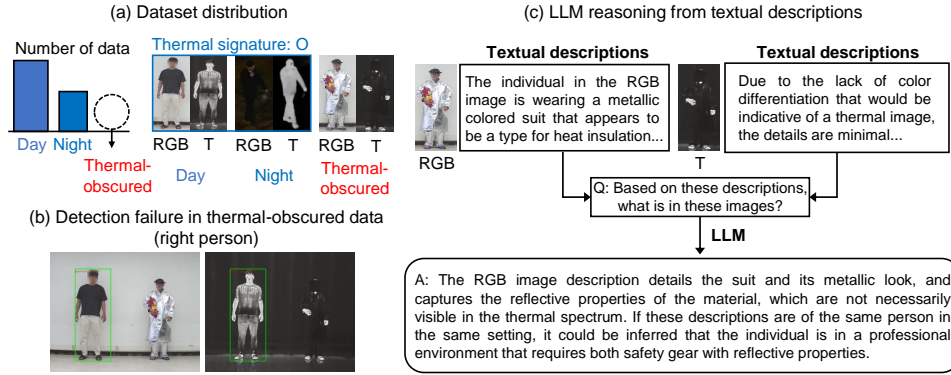


Fig. 1. Problem illustration and our motivation. (a) In multispectral pedestrian datasets, thermal signatures always appear on pedestrians, as the thermal modality can generally capture pedestrians all day/night. In these datasets, thermal-obscured data is underrepresented. Models trained on such datasets learn the statistical co-occurrences between pedestrians and their thermal signatures. (b) As a result, models fail to detect pedestrians in thermal-obscured data, even though obviously visible in RGB. (c) An example of prompting the LLM. Based on the textual descriptions of RGB and thermal images, we prompt the ChatGPT [38] to answer the question “Based on these descriptions, what is in these images?”. The ChatGPT detects the person without suffering modality biases, realizing that a person wearing heat-insulation clothing is invisible in thermal images due to the reflective material. Our motivation is to develop MSCoT prompting based on LLMs and integrate it into vision-based multispectral pedestrian detectors.

LLMs’ rationale-based inference mechanisms for multispectral pedestrian detection. Specifically, by generating detection scores grounded in physical rationales through Chain-of-Thought prompting [37], we can integrate these scores into multispectral pedestrian detectors to help mitigate modality biases and enhance detection accuracy.

To this end, we design the Multispectral Chain-of-Thought (MSCoT) prompting, which prompts the LLM to perform the task of multispectral pedestrian detection. For the inputs of MSCoT prompting, we obtain textual descriptions of pedestrians in both RGB and thermal images from a pre-trained multi-modal language model (MLLMs) [35]. Our goal of MSCoT prompting is to produce probabilistic detection scores from these textual descriptions. However, LLMs are known for their overconfidence [39]–[41] and output confidence scores irrelevant to the context [42]. To overcome this problem, we designed MSCoT prompting to conduct two consecutive Chain-of-Thought [37] (CoT) prompting steps. MSCoT prompting first outputs uni-modal confidence scores and comprehends them with the text of both modalities to produce final detection scores. From these processes, MSCoT prompting facilitates LLMs to produce reliable detection scores that are compatible with multispectral pedestrian detectors.

Building on our MSCoT prompting, we propose the MSCoTDet framework that produces unbiased detections from a statistically biased train set. This problem formulation is adopted rather than explicitly modifying the training priors (such as adding thermal-obscured pedestrians in the train set) to verify that MSCoT prompting can effectively intervene in the modality bias of multispectral pedestrian detectors. Specifically, the MSCoTDet framework integrates the decision processes of MSCoT prompting into vision-based multispectral pedestrian detectors. A Language-driven Multi-modal Fusion (LMF) is designed to effectively integrate these two distinct decision processes.

To evaluate the effectiveness of MSCoTDet, we conduct experiments on generic multispectral pedestrian datasets (FLIR [31], and CVC-14 [32]) and a dataset (ROTX-MP [17]) that mainly contains thermal-obscured pedestrians. Extensive

experiment results show that MSCoTDet generalizes well on ROTX-MP even with biased training data while performing robustly on generic datasets.

Contributions. In summary, our contributions are:

- 1) We propose the Multispectral Chain-of-Thought (MSCoT) prompting strategy, which prompts the LLM to perform the task of multispectral pedestrian detection.
- 2) We propose the MSCoTDet framework, which integrates MSCoT prompting into vision-based multispectral pedestrian detectors.
- 3) Extensive experiments demonstrate that our proposed MSCoTDet framework can significantly intervene in modality bias and improve the overall performance of multispectral pedestrian detectors.

II. RELATED WORK

A. Multispectral Pedestrian Detection

Multispectral pedestrian detection is the task of locating pedestrians in the input image based on multiple visual modalities (i.e., RGB and thermal). It is different from multispectral person re-identification [43] which focuses on matching the same identity across a gallery of images to the query image of the opponent modality. Multispectral person re-identification lacks the detection process, and multispectral pedestrian detection does not consider identity-matching. Moreover, multispectral pedestrian detection stands apart from the task of person search [44] which combines both detection and re-identification, aiming to simultaneously locate and identify a person from input images.

Dataset. Different from standard pedestrian detection [45]–[51], multispectral pedestrian detection aims to detect pedestrians using RGB and thermal images. One challenge in multispectral pedestrian detection is the lack of data. The process of aligning RGB and thermal images requires expensive hardware, such as a beam-splitter [13] and a GPS clock. For annotating bounding boxes of multispectral data, each modality needs separate annotations.

The KAIST [13] dataset is one of the first benchmarks for multispectral pedestrian detection, containing well-aligned

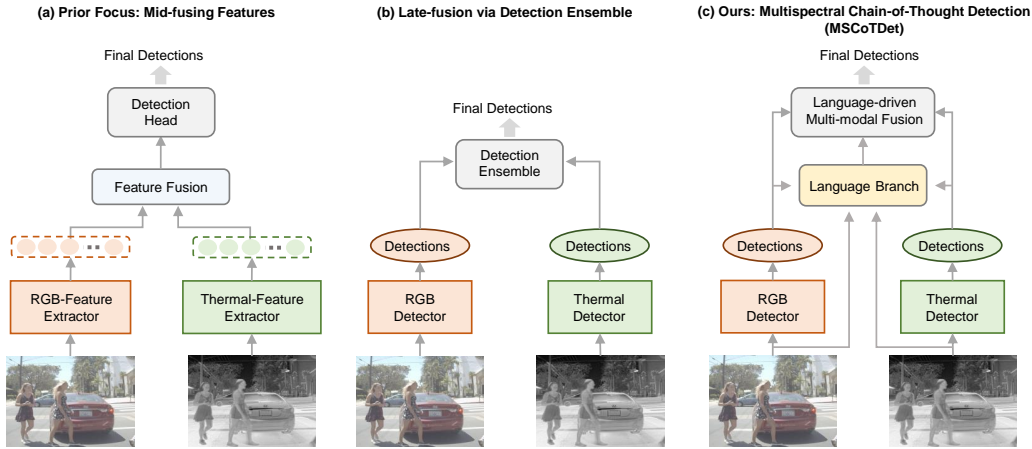


Fig. 2. Comparisons between previous works and our method (MSCoTDet). (a) Previous approaches centrally focused on mid-fusion methods, e.g., mid-fusing features internally in the network. (b) There are few works via late fusion that ensemble detections from independently trained single-modal detectors, i.e., RGB and thermal detectors. (c) MSCoTDet (Ours) focuses on designing a language branch that processes detection using Large Language Models (LLMs). The language branch includes the MSCoT prompting, which prompts the LLM to perform multispectral pedestrian detection. Then, our proposed Language-driven Multi-modal Fusion (LMF) enables fusing vision-driven and language-driven detections.

RGB and thermal images. The FLIR [31] data offers higher image resolution than KAIST [13]. On the other hand, the CVC-14 [32] dataset largely contains misaligned RGB-thermal images. ROTX-MP [17] dataset highlights the challenge due to the dataset bias of multispectral data. ROTX-MP adopts the evaluation setting where the test distribution is significantly different from the training priors. Performing unbiased inference with biased training data remains a challenge in multispectral pedestrian detection.

Models. Previous studies focused on developing various fusion methods for multispectral pedestrian detection. These approaches are based on early-fusion, mid-fusion, or late-fusion, which are often categorized by the fusion stage of the network. Early-fusion [16] methods concatenate RGB and thermal images at the input stage and processes through the detection network. Mid-fusion [5], [12], [16], [18] has been the prior focus, which encodes RGB images and thermal images to the same feature space and fuses them inside the network. However, early-fusion and mid-fusion are known to memorize the training priors and exhibit poor generalizability [17] on out-of-distribution data. Lastly, late-fusion [19], [52] methods are based on ensembling detection results produced from RGB and thermal single-modal detectors. Most of them do heuristic weighting with single-modal detectors or perform simple Bayesian estimation, leading to reduced accuracy.

Specifically, Kim et al. [12] devised an uncertainty-aware multispectral pedestrian detection framework that focuses on reducing the effect of the predictive uncertain modality (e.g., modality with corruption). The stable multispectral pedestrian detection (SMPD) [15] model exploits the Dirichlet distribution to estimate the uncertainty distribution of different modalities and obtain fusion evidence by the Subjective Logic framework. Different from the uncertainty-based models [12], [15], our work utilizes a large language model (LLM) to estimate the modal reliability. This is based on our observations that LLMs offer accurate modal reliability when the descriptions of the modalities are given as texts. ProbEn [19] probabilistically

ensembles detection results obtained from single-modal detectors of different modalities. As ProbEn’s effectiveness depends on accurate probability distributions from both modalities, its effectiveness is degraded if one modality provides highly uncertain or miscalibrated predictions. MSCoTDet mitigates such problems by instructing the LLM to generate detection scores, which can make informed predictions based on the more reliable modality.

MS-DETR [53] expands the DETR architecture [54] from a single-modal detection into the multispectral setting by devising a multi-modal transformer decoder. Compared to MS-DETR [53], MSCoTDet introduces a Language-driven Multi-modal Fusion strategy that combines single-modal DETR models with the inference mechanisms of a large language model (LLM). Lastly, the Causal Mode Multiplexer (CMM) [17] framework aims to learn the causality between multispectral inputs and predictions using counterfactual interventions. However, such a method involves subtracting the direct effect from the model’s detection score, resulting in low confidence levels. MSCoTDet facilitates LLMs to produce detection scores with robust confidence levels using Chain-of-Thought (CoT) Prompting [37] mechanisms.

B. Addressing Modality Biases in Multimodal Learning

As modality biases significantly influence the reliability of multi-modal models, several endeavors have been devoted to solving modality bias issues in different multi-modal tasks such as classification [55], visual question answering (VQA) [33], and person re-identification [56]. One straightforward approach to mitigate modality bias is to augment the training data or use additional annotations. In particular, counterfactual generation [57]–[60] helps to balance the training data by explicitly adding the out-of-distribution priors. However, in the real world, unknown test cases are prevalent, and augmenting all these cases is difficult due to the vast diversity of real-world data [17], [33]. Therefore, various

benchmarks (e.g., VQA-CP [61], ROTX-MP [17]) were proposed to evaluate whether multimodal models generalize well in subtly different distributions from training data.

Under these benchmarks, Wang et al. [55] proposed Gradient Blending, which combines gradient estimates by calculating optimal weights for each modality. Gat et al. [62] leverages the log-Sobolev inequality to bound the functional entropy, effectively maximizing the utilization of each modality's information during training. Niu et al. [33] capture the language bias in the VQA task as the natural direct effect of questions on answers. The debiasing is achieved by subtracting the language bias from the total effect. Similarly, our previous work [17] aims to mitigate the thermal modality bias in multispectral pedestrian detection through counterfactual intervention. They subtract the detection score of the direct thermal path from the total detection score. Different from previous methods that regularize modality's gradients [55], [62] or apply counterfactual intervention [17], [33], our MSCotDet introduces an innovative approach utilizing language and chain of thought. MSCotDet mitigates modality bias by fusing modalities based on the semantic context between multimodal inputs and outputs using LLMs, making it robust to out-of-distribution data.

C. Vision Tasks with LLMs

Large language models (LLMs) excel in natural language processing (NLP) and generation by training on vast amounts of text data [63]–[68]. These features and advantages offer innovative applicability across more general areas of intelligence, such as computer vision. Yang et al. [69] introduced LLM-guided concept bottlenecks (LaBo) for image classification. LaBo generates candidate concepts from GPT-3 [64] and align them to test images by computing similarity scores. Naeem et al. [70] enhance zero-shot image classification framework utilizing an LLM to create web-scale documents. They compute the multiple complementary views of each class between text and image features and perform image classification. Khan et al. [71] improve VQA models by annotating unlabeled images with an LLM.

Park et al. [25] proposed a pedestrian detection framework that integrates LLM-derived text features via clustering and task-prompting. They create a document of pedestrian appearance descriptions using an LLM and combine them with visual features inside the pedestrian detection network. Although previous methods have enhanced model performance using LLMs, they 1) create large documents with LLMs [25], [64], [70], 2) combine/compare text and image features internally in the network [25], [64], [70], or 3) augment training data [71]. Different from previous works, we focus on prompting the LLM to perform the vision task (i.e., multispectral pedestrian detection) so that it fully exploits its linguistic capabilities. Furthermore, our proposed method completely sidesteps the need for constructing large documents or collecting/augmenting additional data.

III. PRELIMINARIES

Before introducing our method, we review the late-fusion strategies in multispectral pedestrian detection. Then we elaborate on our proposed method.

A. Late-fusion in Multispectral Pedestrian Detection

Rather than fusing modalities in the input stage (early-fusion [72]–[74]) or in the intermediate steps (mid-fusion [12], [18]), late-fusion [19], [75] is based on detection ensembling, i.e., fusing the decision values. One of the advantages of late fusion is that it can preserve single-modal models and, therefore, has high flexibility to perform multi-modal fusion from diverse models of different modalities [75]–[80], e.g., *fusing predictions between LLMs and vision-based detectors*. Late fusion methods have been also investigated in multispectral pedestrian detection [19]. They first train single-modal detectors (i.e., RGB and thermal) and then fuse the prediction scores (score fusion) and bounding boxes (box fusion) which are the outputs from single-modal detectors. The final output includes fused prediction scores and bounding boxes. We describe score fusion and box fusion strategies below.

Score Fusion. The most common strategies to fuse prediction scores obtained from single-modal models are averaging [5], [6], Non-maximum Suppression (NMS) [19], and Probabilistic Ensembling (ProbEn [19]). Between them, we adopt averaging and NMS, as we find them effective for our method (Section IV-D). Averaging is straightforward, the fused score is determined by averaging prediction scores estimated in each modality. Denote s_{RGB} and s_T the prediction scores predicted for the same object in different modalities (i.e., RGB and thermal). Then the averaging score fusion between s_{RGB} and s_T can be expressed as:

$$s_{AVG} = \frac{s_{RGB} + s_T}{2}, \quad (1)$$

where s_{AVG} denotes the fused score. On the other hand, NMS compares the prediction scores estimated in each modality and votes for the highest one, removing the lower scores. NMS score fusion between s_{RGB} and s_T can be expressed as:

$$s_{NMS} = \max(s_{RGB}, s_T), \quad (2)$$

where s_{NMS} denotes the fused score by the NMS.

Box Fusion. Box fusion is to merge overlapping bounding boxes predicted from different modalities (i.e., RGB and thermal). Chen et al.(2022) [19] suggests a simple and effective way to probabilistically fuse boxes, which computes a weighted average of boxes. The weights are given by the prediction scores, implying that more confident detections should have a higher weight when fusing boxes. Denote b_{RGB} and b_T the bounding box coordinates predicted for the same object in different modalities (i.e., RGB and thermal). Using the predictions scores s_{RGB} , and s_T , the weighted-averaging box fusion between b_{RGB} and b_T can be expressed as:

$$b_{s-avg} = \frac{b_{RGB} \times s_{RGB} + b_T \times s_T}{s_{RGB} + s_T}, \quad (3)$$

where b_{s-avg} denotes the fused bounding boxes.

Our Motivation. Previous works have studied late-fusion approaches in multispectral pedestrian detection with two single-modal detectors, i.e., an RGB object detector and a thermal object detector. Most do heuristic weighting with single-modal detectors or perform simple Bayesian estimation [19]. Therefore, these methods sometimes neglect

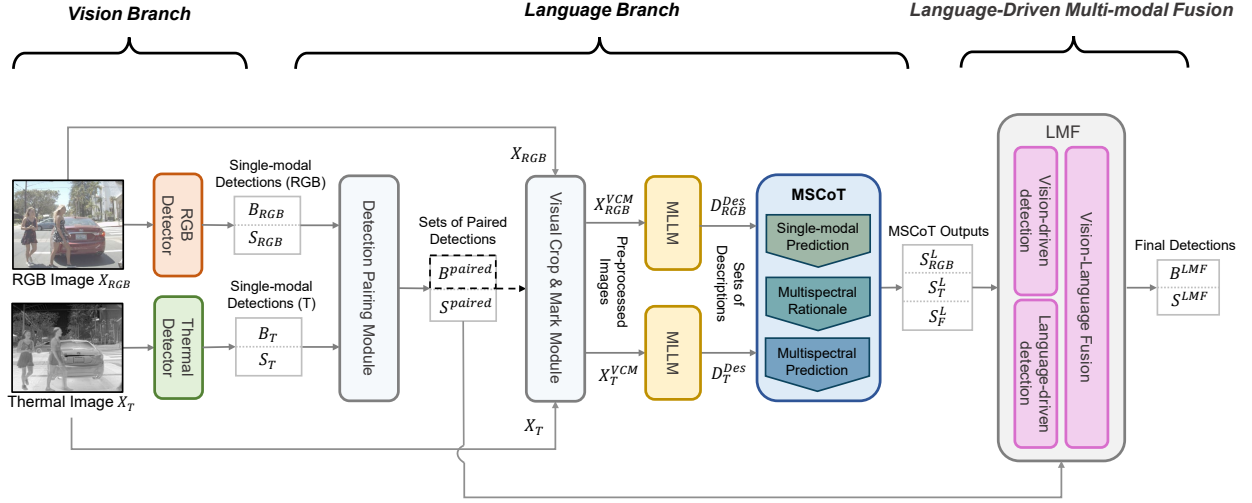


Fig. 3. Overall architecture of proposed Multispectral Chain-of-Thought detection (MSCoTDet) framework including vision branch, language branch, and Language-driven Multi-modal Fusion.

the inter-modality contexts that might differ between the diverse scenarios of multispectral pedestrian detection. One advantage of late-fusion is that it preserves the single-modal predictions, as it does not require aligning different modalities in the same domain (early-fusion) or feature space (mid-fusion). Our motivation is to leverage the late-fusion strategies to fuse predictions from LLMs and vision-based detection models. To this end, we design the Language-driven Multi-modal Fusion (LMF) in Section IV-D. In the next section, we propose the MSCoTDet framework and describe its details.

IV. PROPOSED METHOD

A. Overall Architecture

The overall architecture of our proposed MSCoTDet framework is shown in Fig. 3. It consists of two branches that perform distinct detection processes, the vision branch and the language branch. Detections from these branches are fused to output final detections. We briefly introduce the process of each branch and our fusion strategy.

Vision branch. Given the input of RGB and thermal images X_{RGB} and X_T , the vision branch first produces single-modal (i.e., RGB or thermal) detections. Denote the prediction scores as S_{RGB} , S_T and bounding boxes as B_{RGB} , B_T produced from each single-modal detector. The single-modal detections in the vision branch are processed through the language branch.

Language Branch. The language branch first generates text descriptions of pedestrians and performs detections based on them. Toward this goal, we leverage Multi-modal Large Language Models (MLLMs), which are capable of generating comprehensive descriptions in both RGB and thermal images. Based on these descriptions, we propose the Multispectral Chain-of-Thought (MSCoT) prompting, which prompts the LLM to conduct reasoning steps and produce detections (Section IV-C). Detections from MSCoT prompting include single-modal (i.e., RGB and thermal) prediction scores S_{RGB}^L , S_T^L , and fused prediction scores S_F^L . In Sections IV-B and IV-C, we describe the processes to produce these detections in detail.

Language-driven Multi-modal Fusion (LMF). Vision-driven detection, language-driven detection, and vision-language fusion are performed to produce final detections, S_{LMF} and B_{LMF} . In Section IV-D, we describe the fusion strategies in detail.

B. Cross-modal Pedestrian Description Generation

The first step of the language branch is to generate text descriptions of pedestrians, both from the RGB and thermal images. We prompt a Multi-modal Large Language Model (MLLM) ChatGPT-4V [35] to describe pedestrian regions in the image, which can be identified by their bounding box coordinates B_{RGB} , B_T obtained from single-modal detectors. However, there are two challenges, which we introduce below with their solutions.

Detection Pairing. The first challenge is due to the misalignment in multispectral data [12], [13]. The same pedestrian often appears in different locations within the RGB and thermal image pairs, as their image sensors may have different Field-of-View or frame rates [12]. In such cases, we need to guide MLLMs to make descriptions based on different image regions in RGB and thermal images for the same pedestrians. Our strategy is to find the detection pairs from the single-modal detections (e.g., bounding boxes) that belong to the same pedestrians and provide this information to the MLLM.

Although bounding boxes representing the same pedestrian can have different coordinates in different modalities, still they will contain highly overlapping areas in the images, and those boxes will have large values of IoUs (Intersection-of-Unions). Specifically, for the i -th bounding box $b_{i,m}$ in bounding boxes B_m , obtained from the single-modal detector in the m modality (m is either RGB or thermal: T), we aim to find the bounding box from B_{m^c} , in the opposite modality m^c that corresponds to the same pedestrian. To this end, we compute the IoU value between $b_{i,m}$ across all bounding boxes in B_{m^c} , and find the box that has the highest IoU value, e.g.,

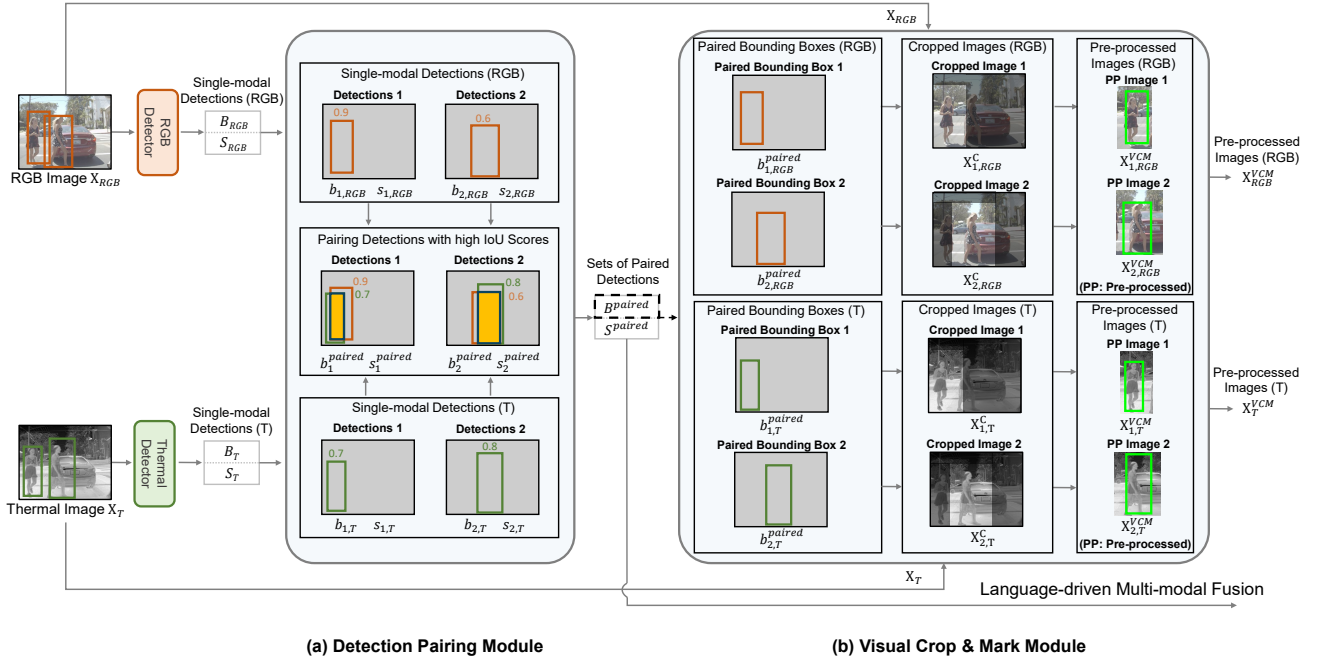


Fig. 4. Visualized details of the (a) Detection Pairing Module and the (b) Visual Crop & Mark Module. (a) The Detection Pairing Module gets single-modal detections from the vision branch and then finds the detection pairs that belong to the same pedestrians, e.g., $b_1^{paired} = (b_{1,RGB}^{paired}, b_{1,T}^{paired})$ and $s_1^{paired} = (s_{1,RGB}^{paired}, s_{1,T}^{paired})$. Through the iteration of pedestrians, the module produces the sets of paired detections B^{paired} and S^{paired} . (b) The Visual Crop & Mark Module gets B^{paired} as inputs, and output the pre-processed images X_{RGB}^{VCM} and X_T^{VCM} .

Algorithm 1: Detection Pairing (DPair)

- 1: **Input:** Prediction scores S_{RGB} , S_T , Bounding boxes B_{RGB} , B_T .
 - 2: **Require:** An IoU threshold τ .
 - 3: **Output:** Paired bounding boxes B^{paired} , paired prediction scores S^{paired} .
 - 4:
 - 5: **procedure** DPair($B_{RGB}, B_T, S_{RGB}, S_T; \tau$)
 - 6: **initialize** lists $B \leftarrow B_{RGB} \cup B_T$, $S \leftarrow S_{RGB} \cup S_T$, $B^{paired} \leftarrow \phi$, and $S^{paired} \leftarrow \phi$.
 - 7: Find the box $b_{max} \in B$ of the highest prediction score.
 - 8: Find boxes $D \in B$ overlapping with b_{max} , of IoU ($> \tau$) in the opposite modality.
 - 9: Find the box $b_{pair} \in D$ of the highest IoU value.
 - 10: If D is empty, then $b_{pair} \leftarrow b_{max}$ and $s_{pair} \leftarrow s_{max}$.
 - 11: Append (b_{max}, b_{pair}) to B^{paired} .
 - 12: Append (s_{max}, s_{pair}) to S^{paired} .
 - 13: Remove b_{max} and b_{pair} from B and s_{max} and s_{pair} from S .
 - 14: Repeat this process until B and S are empty.
 - 15: **return** B^{paired} , S^{paired}
 - 16: **end procedure**
-

b_{j,m^c} , with $b_{i,m}$. Here, we only consider the boxes with IoU values above the IoU threshold τ . With indices i and j , we can find a pair of the prediction scores $s_{i,m}$ and s_{j,m^c} that belong to the same pedestrian. We call such tuples $(b_{i,m}, b_{j,m^c})$ and $(s_{i,m}, s_{j,m^c})$ as the “paired detection”. When all IoU values are under the IoU threshold τ , this means that there are no boxes in B_{m^c} that correspond to the same pedestrian and $b_{i,m}$ can not find a pair. Such cases can occur at nighttime or in thermal-obscured scenarios where the pedestrian is detected by

Algorithm 2: Visual Crop & Mark (VCM)

- 1: **Input:** An image X , and bounding boxes B .
 - 2: **Output:** Pre-processed images X^{VCM} .
 - 3:
 - 4: **procedure** VCM(X, B)
 - 5: **initialize** $X^{VCM} \leftarrow \phi$.
 - 6: **for** all bounding boxes b in B
 - 7: Draw a green box at bounding box b in the image X .
 - 8: Crop the image X around the bounding box b such that the width and height of the cropped image X_c are twice as the width and height of b .
 - 9: Append the cropped image X_c to X^{VCM} .
 - 10: **end for**
 - 11: **return** X^{VCM}
 - 12: **end procedure**
-

only one modality. In this case, we override the value of $b_{i,m}$ and $s_{i,m}$ to the opposite modality, making pairs of $(b_{i,m}, b_{i,m})$ and $(s_{i,m}, s_{i,m})$. Iterating this process for over all bounding boxes in B_m and B_{m^c} (i.e., B_{RGB} and B_T) allows us to obtain a set of paired detections B^{paired} and S^{paired} . Denote the Detection Pairing Module as a function $DPair(\cdot)$ with respect to inputs B_{RGB} , B_T , S_{RGB} , and S_T , which indicate bounding boxes and prediction scores obtained from RGB and thermal single-modal detectors, respectively. The inputs and outputs of $DPair(\cdot)$ can be represented as:

$$S^{paired}, B^{paired} = DPair(B_{RGB}, B_T, S_{RGB}, S_T; \tau), \quad (4)$$

where τ indicates an IoU threshold. We set this value to 0.5, the standard value used in the object detection task.

Algorithm 3: Cross-aligned Pedestrian Description Generation (CPDG)

```

1: Input: An RGB image  $X_{RGB}$ , an thermal image  $X_T$ ,
   prediction scores  $S_{RGB}$ ,  $S_T$  and bounding boxes  $B_{RGB}$ ,  $B_T$ .
2: Require: Input text prompts  $p_{RGB}$ ,  $p_T$ , and IoU threshold  $\tau$ .
   Detection pairing module  $DPair(\cdot)$ , Visual Crop & Mark
   module  $VCM(\cdot)$ . A pre-trained multimodal large language
   model  $MLLM(\cdot)$ .
3: Output: A set of RGB descriptions  $D_{RGB}$ , a set of thermal
   descriptions  $D_T$ , and paired detections  $S^{paired}$ ,  $B^{paired}$ .
4:
5: procedure CPDG( $X_{RGB}, X_T, S_{RGB}, S_T, B_{RGB}, B_T$ ,
    $p_{RGB}, p_T, \tau$ )
6:    $S^{paired}, B^{paired} \leftarrow DPair(B_{RGB}, B_T, S_{RGB}, S_T; \tau)$ .
7:    $X_{RGB}^{VCM} \leftarrow VCM(X_{RGB}, B^{paired})$ .
8:    $X_T^{VCM} \leftarrow VCM(X_T, B^{paired})$ .
9:   initialize list  $D_{RGB} \leftarrow \phi$ ,  $D_T \leftarrow \phi$ .
10:  for all images  $x_{RGB}^{VCM}$  in  $X_{RGB}^{VCM}$ 
11:     $d_{RGB} \leftarrow MLLM(x_{RGB}^{VCM}; p_{RGB})$ .
12:    Append the text description  $d_{RGB}$  to  $D_{RGB}$ .
13:  end for
14:  for all images  $x_T^{VCM}$  in  $X_T^{VCM}$ 
15:     $d_T \leftarrow MLLM(x_T^{VCM}; p_T)$ .
16:    Append the text description  $d_T$  to  $D_T$ .
17:  end for
18:  return  $D_{RGB}, D_T, S^{paired}, B^{paired}$ .
19: end procedure

```

B^{paired} is used to guide MLLMs the location of when making descriptions in RGB and thermal images. S^{paired} is used when fusing prediction scores from vision and language branches in Section IV-D. The complete algorithm of the Detection Pairing Module is described in Algorithm 1.

Visual Crop & Mark (VCM). Another challenge when using MLLMs for making descriptions is the low accuracy of MLLMs on small-scale objects, i.e., objects occupying a small area in the image. To solve this issue, we refer to a recent method [81] that improves the performance of MLLMs on small visual details by pre-processing the input image with image cropping. Similarly, we zoom in on the target pedestrians and crop the image around it, such that visual information irrelevant to the pedestrian is removed. We find such a pre-processing strategy is shown to significantly improve the accuracy of MLLMs in describing small-scale pedestrians, near the level comparable to recognizing large-scale pedestrians.

The detailed algorithm for VCM is described in Algorithm 2. First, an image X and bounding boxes B are given as input. Note that B represents the locations of pedestrians in image X . For each bounding box b , the image X is cropped around b so that the width and height of the cropped image X_c are twice as b .

In addition to cropping, we visually guide the MLLM to describe a specific pedestrian by drawing a 1-pixel width “green” color (with RGB values (0,255,0)) box around a target pedestrian. We use the “green” color to draw the boxes because it is most distinctly in hue from human skin color, thus effective for distinguishing humans from the background. This process is iterated for all bounding boxes $b \in B$ for both

a RGB image X_{RGB} and a thermal image X_T . Denote this the Visual Crop & Mark process as $VCM(\cdot)$, then the pre-processed RGB and thermal images X_{RGB}^{VCM} and X_T^{VCM} can be written as:

$$X_{RGB}^{VCM} \leftarrow VCM(X_{RGB}, B^{paired}), \quad (5)$$

$$X_T^{VCM} \leftarrow VCM(X_T, B^{paired}), \quad (6)$$

where X_{RGB} and X_T are RGB and thermal input images, and B^{paired} is the set of the paired bounding boxes. When pre-processing images in X_{RGB} and X_T , bounding boxes of the corresponding modality in B^{paired} are used only.

Generating Descriptions with MLLMs. For each pre-processed image $x_{RGB}^{VCM} \in X_{RGB}^{VCM}$ and $x_T^{VCM} \in X_T^{VCM}$, we prompt the MLLM as the following. For the RGB image, “In this RGB image, what is in the green box?” and for the thermal image, “In this thermal image, what is in the green box?”. Denote these prompts as p_{RGB} , and p_T . Then, we can generate their corresponding text descriptions d_{RGB} and d_T such as:

$$d_{RGB} \leftarrow MLLM(x_{RGB}^{VCM}; p_{RGB}), \quad (7)$$

$$d_T \leftarrow MLLM(x_T^{VCM}; p_T), \quad (8)$$

where $MLLM(\cdot)$ denotes the process of generating text descriptions from an MLLM, given the pre-processed image as input. Text descriptions are generated for all $x_{RGB}^{VCM} \in X_{RGB}^{VCM}$ and $x_T^{VCM} \in X_T^{VCM}$, producing sets of descriptions D_{RGB} and D_T . The detailed algorithm for Cross-modal Pedestrian Description Generation (CPDG) is described in Algorithm 3.

C. Multispectral Chain-of-Thought Prompting

We introduce Multispectral Chain-of-Thought (MSCoT) prompting, which facilitates LLMs to build step-by-step cross-modal rationales and produce detection results. MSCoT prompting first comprehends intra-modality information and produces single-modal prediction scores from each RGB and thermal description. Then, MSCoT prompting comprehends inter-modality reasoning and outputs fused detection scores and bounding boxes. This multi-step reasoning process addresses LLMs’ overconfidence [39] and produce calibrated confidence scores.

To this end, we refer to the Chain-of-Thought (CoT) prompting [37] technique, which significantly improves LLM’s reasoning ability in complex NLP tasks. CoTs add a series of intermediate reasoning steps into LLMs and generate rationales when predicting answers. Motivated by the late-fusion process in multispectral pedestrian detection, we propose a Multispectral Chain-of-Thought (MSCoT) prompting chain.

Given the text descriptions $d_{RGB} \in D_{RGB}$ and $d_T \in D_T$ of a RGB image and a thermal image, MSCoT prompting first prompts the LLM to produce single-modal prediction scores s_{RGB}^L , and s_T^L and then predict a fused prediction score s_F^L based on rationale chains. Given the descriptions d_{RGB} , and d_T of RGB and thermal images as the context, we design the following prompt chains.

Generating Single-modal Prediction.

Given the RGB image description d_{RGB} and the thermal

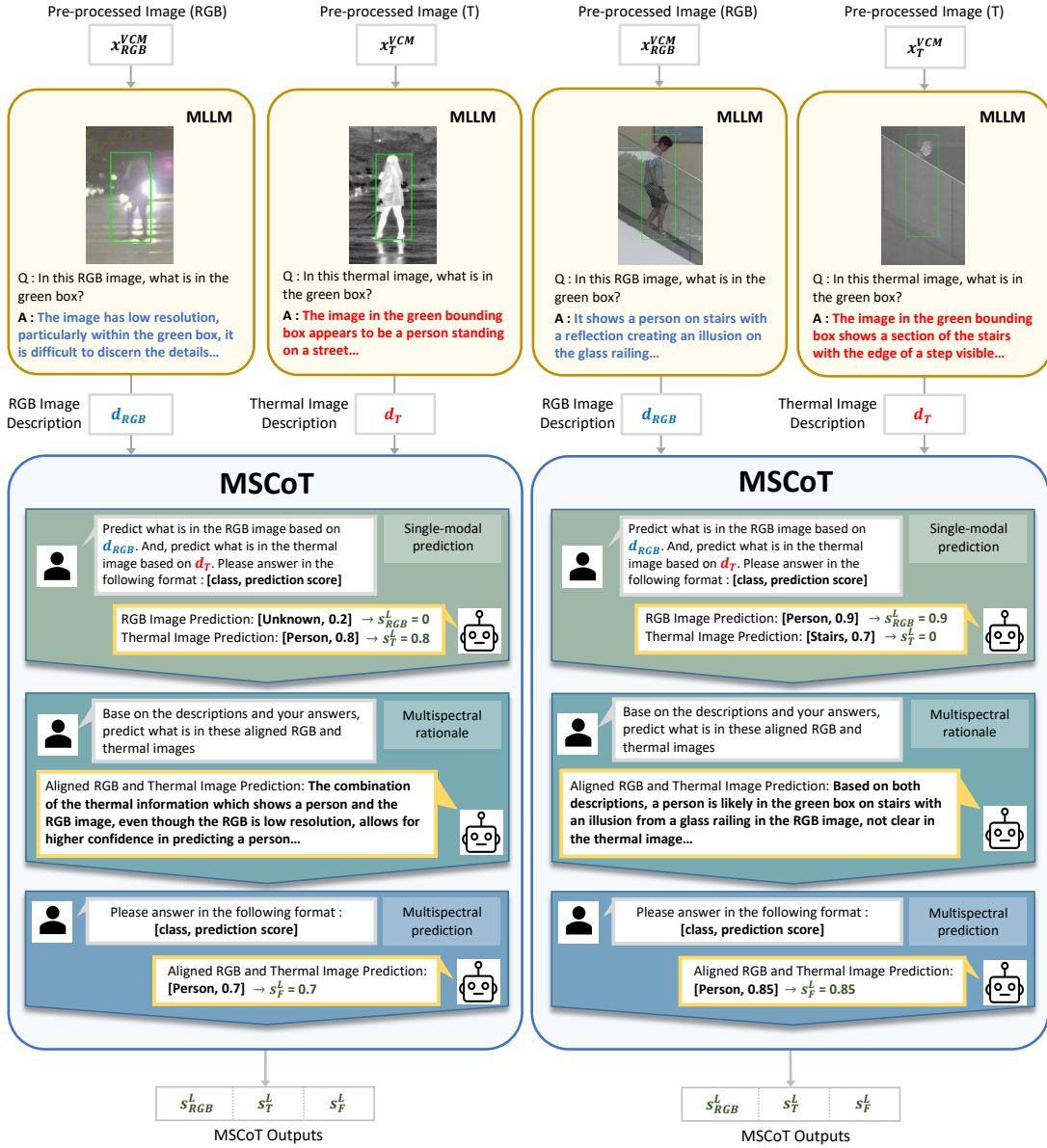


Fig. 5. Visualized process of our proposed Multispectral Chain-of-Thought (MSCoT) prompting.

image description d_T , the LLM is prompted with context $[d_{RGB} \ d_T]$ and text prompt p_{single} as the following (line 8 in Algorithm.4).

Context $[d_{RGB} \ d_T]$: RGB image description d_{RGB} , thermal image description d_T .

Prompt p_{single} : First, predict what is in the RGB image based on d_{RGB} . And predict what is in the thermal image based on d_T . Please answer in the format : [class, prediction score]

From the above prompt, the LLM outputs $\{[c_{RGB}^L, s_{RGB}^L], [c_T^L, s_T^L]\}$, including single-modal prediction scores s_{RGB}^L, s_T^L and class labels c_{RGB}^L, c_T^L (line 8 in Algorithm. 4). s_{RGB}^L, s_T^L are assigned zero if c_{RGB}^L, c_T^L are not “person”, respectively (line 9-10 in Algorithm. 4).

Generating Multispectral Rationales and Prediction.

Additionally providing s_{RGB}^L , and s_T^L as the context, the LLM is prompted to generate multispectral rationales and fused predictions. Given the RGB image description d_{RGB} , the thermal image description d_T , and answers s_{RGB}^L, s_T^L of the single-modal predictions, the LLM is prompted with the context $[d_{RGB} \ d_T \ s_{RGB}^L \ s_T^L]$ and text prompt p_{multi} as the following (line 12 in Algorithm.4).

Context $[d_{RGB} \ d_T \ s_{RGB}^L \ s_T^L]$: RGB image description: d_{RGB} , thermal image description: d_T , answers: s_{RGB}^L , and s_T^L . Prompt p_{multi} : Based on the descriptions and your answers, predict what is in these aligned RGB and thermal images. Please answer in the format: [class, prediction score]

From the above prompt, the LLM outputs $[c_F^L, s_F^L]$, including fused prediction score s_F^L and class label c_F^L (line 12 in Algorithm. 4). s_F^L , is assigned zero if c_F^L is not “person”.

Algorithm 4: Multispectral Chain-of-Thought (MSCoT) Prompting

```

1: Input: RGB image description  $d_{RGB}$ , and thermal image
   description  $d_T$ .
2: Require: A pre-trained large language model  $LLM(\cdot)$ ,
3: text prompts  $p_{single}$  and  $p_{multi}$ .
4: Output: RGB single-modal prediction score  $s_{RGB}^L$ , thermal
   single-modal prediction score  $s_T^L$ , fused prediction score  $s_F^L$ .
5:
6: procedure MSCoT( $d_{RGB}, d_T$ )
7:   # Generate Single-Modal Predictions
8:    $\{[c_{RGB}^L, s_{RGB}^L], [c_T^L, s_T^L]\} \leftarrow LLM([d_{RGB} \ d_T]; p_{single})$ .
9:    $s_{RGB}^L \leftarrow 0$  if  $c_{RGB}^L \neq \text{"person"}$ 
10:   $s_T^L \leftarrow 0$  if  $c_T^L \neq \text{"person"}$ 
11:  # Generate Multispectral Rationales and Predictions
12:   $[c_F^L, s_F^L] \leftarrow LLM([d_{RGB} \ d_T \ s_{RGB} \ s_T]; p_{multi})$ .
13:   $s_F^L \leftarrow 0$  if  $c_F^L \neq \text{"person"}$ 
14:  return  $s_{RGB}^L, s_T^L, s_F^L$ .
15: end procedure

```

(line 13 in Algorithm. 4). s_{RGB}^L , s_T^L , and s_F^L , the outputs of MSCoT Prompting with respect to the inputs d_{RGB} , d_T can be expressed as:

$$s_{RGB}^L, s_T^L, s_F^L = MSCoT(d_{RGB}, d_T). \quad (9)$$

Iterating this process over all $d_{RGB} \in D_{RGB}$ and $d_T \in D_T$ obtains the prediction scores: s_{RGB}^L , s_T^L , and s_F^L . Our implementation for MSCoT prompting is achieved by fine-tuning ChatGPT-3.5 [38] with about 50 training samples. The implementation details are described below. **Finetuning the LLM for MSCoT.** We use the ChatGPT-3.5 (GPT-3.5) API [38], provided by the OpenAI developer platform. Using the fine-tuning module provided on the GPT official website [82], we trained GPT-3.5 API with our training data. The official document for GPT-3.5 [82] recommends training 50 samples for fine-tuning the model, and we utilized a total of 50 training samples for each FLIR and CVC-14 model. The training data contains textual descriptions of RGB and thermal images, rationale, and prediction scores for training the Large Language Model. We prompt the GPT-3.5 [38] consisting of rationale and prediction scores. The following answers are obtained by prompting the GPT-3.5 independently with these prompts, and we merge the answers to make the training data. Then with these data, we fine-tune the model answer based on a chain of prompts. The training data are manually selected with high-quality answers, containing reasonable rationales and confidence scores. 50 training data from the FLIR training images are used for fine-tuning the MSCoT of the FLIR model. Also, we made 50 training data using the CVC-14 training images for MSCoT of the CVC-14 model. Note that images from ROTX-MP are not used for making training data for MSCoT because it violates the evaluation setting for ROTX-MP.

D. Language-driven Multi-modal Fusion (LMF)

We propose to ensemble the detections of the vision branch and the language branch at the last stage of the

proposed network (Fig. 3). The Language-driven Multi-modal Fusion (LMF) consists of three implementation mechanisms: 1) Vision-driven Detection (Eq.10), 2) Language-driven Detection (Eq.11), and 3) Vision-Language Fusion (Eq.12). Vision-driven Detection (Eq.10) and Language-driven Detection (Eq.11) calculate detection scores and bounding boxes separately for each vision and language branch. Vision-Language Fusion (Eq.12) then fuses detection results from the vision branch and the language branch.

Vision-driven Detection. For the vision branch, denote S_{RGB}^V as the prediction scores from S^{paired} , and B_{RGB}^V as the bounding boxes from B^{paired} that corresponds to the RGB modality, similar for S_T^V and B_T^V . Then, the vision-driven detections S_F^V (predictions scores) and B_F^V (bounding boxes) can be produced as:

$$S_F^V = \max(S_{RGB}^V, S_T^V), \quad B_F^V = \frac{B_{RGB}^V \odot S_{RGB}^V + B_T^V \odot S_T^V}{S_{RGB}^V + S_T^V}, \quad (10)$$

where \odot denotes the Hadamard product (element-wise multiplication). NMS (Eq. 2) and weighted-averaging (Eq. 3) are applied for score-fusion and box-fusion.

Language-driven Detection. Next, for the language branch, fused bounding boxes B_F^L can be produced as:

$$B_F^L = \frac{B_{RGB}^V \odot S_{RGB}^L + B_T^V \odot S_T^L}{S_{RGB}^L + S_T^L}, \quad (11)$$

given the bounding boxes B_{RGB}^V , B_T^V obtained single-modal detectors. Weighted-averaging (Eq. 3) is applied for box-fusion. The fused prediction scores S_F^L are produced by the MSCoT prompting (Section IV-C).

Vision-Language Fusion. The LMF fuse detection results from the vision branch and the language branch by Vision-Language Fusion (Eq.12). Vision-Language Fusion is particularly designed to handle potential information asymmetries by weighting the detection scores S_F^V , S_F^L and bounding box coordinates B_F^V , B_F^L obtained from both branches. The final detections are produced as:

$$S_{LMF} = \text{avg}(S_F^V, S_F^L), \quad B_{LMF} = \frac{S_F^V \odot B_F^V + S_F^L \odot B_F^L}{S_F^V + S_F^L}, \quad (12)$$

where S_{LMF} and B_{LMF} denote final prediction scores and bounding boxes. Averaging (Eq. 2) and weighted-averaging (Eq. 3) are applied for score-fusion and box-fusion.

Design Choice. For score-fusion, we adopted the NMS method (Eq. 2) in the vision-driven detection. NMS compares the prediction scores estimated in each modality and votes for the highest one, removing the lower score. We apply such a strategy because higher confidence scores generally occur when there is more useful information for detecting the pedestrian. From this strategy, we can obtain higher prediction scores for true-positive detections in most cases. However, it can also increase the prediction scores for false positives. As MSCoT prompting can comprehend very low prediction scores for false positives, we adopt the averaging strategy (Eq. 1) in the vision-language fusion to refine over-confident false positives from the vision-driven detections. For box-fusion, we adopted the weighting average (Eq. 3) method in all processes,

implying that more confident detections should have a higher weight when fusing. In Section VII-B, we conduct an ablation study on these design choices.

V. EXPERIMENTAL SETUP

A. Dataset and Evaluation Metric

The experiments are conducted on multispectral pedestrian datasets: Teledyne FLIR Free ADAS Thermal Dataset v2.0.0 [31], CVC-14 [32], ROTX-MP [17]. The FLIR [31] dataset consists of RGB and thermal image pairs with an image resolution of 640×512 . For a fair comparison with previous studies [3], [17], [18], [83], we use the aligned version of FLIR, proposed by [83]. This version filters out misaligned images, containing well-aligned 4,129 training and 1,013 test RGB and thermal image pairs. For convenience, we call this version of the dataset as FLIR. We evaluate both day and night images and report the performance on the entire test set ('All'). In contrast to FLIR, the CVC-14 [32] dataset often contains heavily misaligned pairs of RGB and thermal images. The train and test set each contain 3,618 and 1,433 grayscale and thermal images with a 640×471 resolution. We evaluate daytime ('Day'), nighttime ('Night'), and the total ('All') test images separately, following previous works [12], [17]. Lastly, we evaluate our method on the ROTX-MP [17] dataset, which consists of 1,000 test images of mainly thermal-obscured pedestrians. We use the models trained from FLIR and CVC-14 to test on ROTX-MP, as this dataset aims to evaluate multispectral pedestrian detectors when there is a substantial distribution change between the train and test splits. For the evaluation metric, we use the Average Precision (AP \uparrow). These experimental settings are the same as the original paper [17].

B. Implementation Detail

Single-modal Detectors. For the single-modal detectors, we use the Co-DETR [84] model and train RGB images and thermal images separately. Co-DETR is based on the DETR (DEtection TRansformer) [85] architecture, enhanced by collaborative learning with multiple parallel auxiliary heads integrated into the output of the transformer encoder. We train the single-modal detectors with RGB and thermal images from FLIR [31] and CVC-14 [32] training data, respectively. For optimizing Co-DETR, we use the same setting in the original paper [84], using AdamW [86] optimizer with an initial learning rate of $1e-4$ and weight decay of $1e-4$. All models are trained on an eight NVIDIA A6000 GPU for 16 epochs with a batch size of 16.

Large Language Models (LLMs). We use two types of Large Language Models. First is the Multimodal Large Language Model (MLLM), which we use to generate text descriptions for RGB and thermal pedestrian images (Section IV-B). For the MLLM, we use the pre-trained model of the ChatGPT-vision (GPT-4V) [35] API, provided by the OpenAI developer platform.

The second is the chatbot version, ChatGPT-3.5 (GPT-3.5) API [38], also provided by the OpenAI developer platform.

We fine-tuned the GPT-3.5 model for the Multispectral Chain-of-Thought (MSCoT) prompting (Section IV-C) we proposed. Using the fine-tuning module provided on the GPT official website [82], we trained GPT-3.5 API with our high-quality selection pairs consisting of RGB, thermal descriptions, rationale, and prediction scores. The official document for GPT-3.5 [82] recommends training 50 samples for fine-tuning the model, and we utilized a total of 50 training samples.

C. Comparison Model

We compare our method with seven multispectral pedestrian detection models: 1) Halfway Fusion [5], 2) Cross-modality Fusion Transformer (CFT) [18], 3) Kim et al. [12], 4) ProbEn [19], 5) Causal Mode Multiplexer (CMM) [17], 6) ICAFusion [87], and 7) MS-DETR [53]. We used the same experimental settings as their original papers. **Halfway Fusion:** we use the Faster-RCNN [88] as the base model and train the model for 3 epochs. The learning rate is initialized at 0.008 during the initial 2 epochs with SGD [89] and subsequently applied a 0.1 learning rate decay for the final epoch. **CFT:** The initial learning rate is 0.01 with a momentum of 0.937, and weight decay 0.0005. Batch size is 32 and the model is trained for 200 epochs and the YOLO-v5 weight trained on the COCO dataset is used for weight initialization. We used the official code. **Kim et al:** The learning rate is initialized at 0.006 during the initial 2 epochs and a 0.1 learning rate decay was applied for the final epoch. We used the official code. **ProbEn:** We finetune two single-modal detectors based on Faster R-CNN [88] pretrained on COCO [90]. The Detectron 2 [91] library is used. We used SGD [89] optimizer with learning rate $5e-3$. We adopt the 'ProbEn' score fusion and 'v-avg' box fusion because such combinations are shown the most effective in the original paper [19]. Also, we adopt the E+M+T ensemble version, indicating that early-fusion, mid-fusion, and thermal single-modal detectors are ensembles.

CMM [17]: The CMM framework is based on the Uncertainty-guided model [12], with the FPN architecture with ResNet-50 [92]. The learning rate is initialized at 0.007 during the initial 1 epoch and then a 0.1 learning rate decay is applied for the final epoch. The Region of Interests (RoIs) per image is set to $N=300$. We apply switchable Total Indirect Effect (sTIE) for every ROI and compute the prediction score. We used the official code, with the same settings as the original paper [17]. **ICAFusion:** We used the official code provided by the authors. The model is trained for 60 epochs, with a batch size of 8. SGD [89] optimizer is used. The initial learning rate is 1.0×10^{-2} with a momentum value of 0.937. The weight decay factor is 0.0005. The cosine annealing method is used for learning rate decay. **MS-DETR:** We used the code provided by the authors. The model is pretrained on the COCO [90] dataset with the Resnet50 [92] backbone. Transformer encoder and decoder consist of 6 layers. The number of feature scales, sampling points, object queries, and attention heads are $L = 4$, $K = 4$, $N = 300$, and $H = 8$, respectively. Adam [93] optimizer is used. The model is trained for 10 epochs with batch size 2. The initial learning rate is 0.0001 and is reduced by a factor of 10 halfway through the training process.

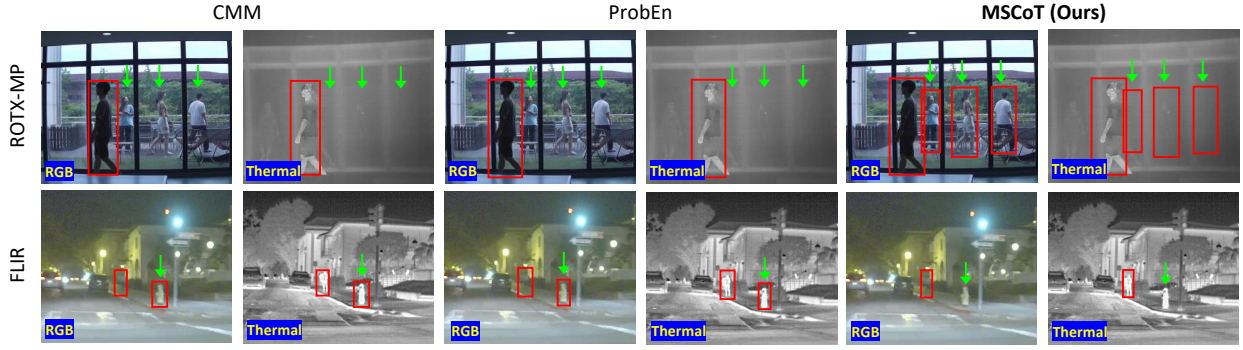


Fig. 6. Visualized detections on the ROTX-MP [17] (Top) and FLIR [31] (Bottom) datasets. (Top): MSCoTDet can detect pedestrians over the window (\downarrow), in which their thermal signatures are absent due to the window. In contrast, other models (CMM [17], ProbEn [19]) fail to detect these pedestrians. (Bottom): Moreover, other models create false-positive detections on the fireplug (\downarrow) due to its thermal signature similar-looking to pedestrians. In contrast, MSCoTDet (Ours) makes correct predictions.

Train	FLIR				CVC-14				Modality Used			Train	FLIR				CVC-14				Modality Used		
Test	FLIR				CVC-14							Test	ROTX-MP				ROTX-MP						
Metric	AP(↑)	MR(↓)			AP(↑)	MR(↓)						Metric	AP(↑)	MR(↓)			AP(↑)	MR(↓)					
Method	All	Day	Night	All	All	Day	Night	All	RGB	Thermal	Language	Method	All	Day	Night	All	All	Day	Night	All	RGB	Thermal	Language
Halfway Fusion [5]	75.85	42.13	36.75	40.65	79.42	36.29	26.29	31.99	✓	✓		Halfway Fusion [5]	36.95	69.76	51.45	59.13	8.80	86.65	94.36	92.01	✓	✓	
CFT [18]	84.10	17.32	22.42	21.26	88.45	18.81	25.25	21.83	✓	✓		CFT [18]	3.64	81.51	87.68	83.83	8.58	98.01	89.89	94.38	✓	✓	
Kim et al. [12]	84.67	20.29	18.72	20.81	90.08	23.87	11.08	18.70	✓	✓		Kim et al. [12]	21.69	63.99	60.68	64.02	13.36	73.54	98.75	84.49	✓	✓	
CMM [17]	87.80	17.81	13.01	16.60	90.47	27.81	7.71	17.13	✓	✓		CMM [17]	57.09	32.23	33.19	33.63	34.96	48.47	51.16	53.39	✓	✓	
ProbEn [19]	86.74	21.29	10.16	17.45	88.31	23.01	21.02	23.23	✓	✓		ProbEn [19]	17.20	72.47	67.88	69.04	16.66	67.24	76.78	73.40	✓	✓	
ICAFusion [87]	86.80	19.39	14.46	17.92	88.43	25.88	14.32	18.99	✓	✓		ICAFusion [87]	44.63	38.58	59.92	47.10	28.16	53.63	63.18	56.63	✓	✓	
MS-DETR [53]	88.08	17.27	10.44	15.37	90.79	24.10	8.80	16.90	✓	✓		MS-DETR [53]	54.77	27.96	40.95	35.33	15.32	75.42	75.70	76.24	✓	✓	
Halfway Fusion [5] + LLM	69.82	48.39	41.74	46.47	78.14	38.11	31.75	35.75	✓	✓	✓	Halfway Fusion [5] + LLM	32.88	65.47	62.63	65.59	6.84	95.18	94.10	94.65	✓	✓	✓
CFT [18] + LLM	83.97	16.65	26.54	23.91	87.89	17.01	30.12	23.81	✓	✓	✓	CFT [18] + LLM	0.95	95.38	95.37	95.34	2.90	97.37	98.36	97.45	✓	✓	✓
Kim et al. [12] + LLM	84.26	19.17	20.95	21.37	89.47	30.90	10.61	20.49	✓	✓	✓	Kim et al. [12] + LLM	19.17	65.82	65.23	66.61	12.65	82.38	89.79	87.11	✓	✓	✓
CMM [17] + LLM	87.79	18.85	13.27	17.85	91.39	22.82	8.47	15.61	✓	✓	✓	CMM [17] + LLM	37.39	42.89	45.71	44.34	37.93	40.57	45.04	43.10	✓	✓	✓
ProbEn [19] + LLM	89.38	16.72	10.08	14.56	89.50	15.29	24.33	19.97	✓	✓	✓	ProbEn [19] + LLM	24.55	61.38	64.09	62.75	23.56	62.17	53.65	59.45	✓	✓	✓
ICAFusion [87] + LLM	86.01	20.46	14.45	18.56	88.51	24.95	13.21	18.38	✓	✓	✓	ICAFusion [87] + LLM	44.00	39.75	61.16	48.12	21.78	55.36	67.81	65.37	✓	✓	✓
MS-DETR [53] + LLM	87.64	17.61	10.89	15.68	90.64	26.12	9.27	18.30	✓	✓	✓	MS-DETR [53] + LLM	30.28	43.49	54.23	55.24	9.74	90.64	89.77	90.11	✓	✓	✓
MSCoTDet(Ours)	90.39	13.99	8.38	12.16	92.38	6.69	13.69	10.39	✓	✓	✓	MSCoTDet(Ours)	67.33	15.23	24.02	23.57	57.65	27.16	34.35	34.18	✓	✓	✓

TABLE I

DETECTION PERFORMANCE ON THE FLIR [31], CVC-14 [32] (LEFT), AND ROTX-MP [17] (RIGHT). (LEFT): WE TRAIN AND TEST ON FLIR, CVC-14 DATASETS. (RIGHT): WE TRAIN MODELS ON FLIR, CVC-14, AND EVALUATE MODELS ON THE ROTX-MP DATASET. WE ADOPT THIS EXPERIMENTAL SETTING FOLLOWING THE ORIGINAL PAPER [17] TO EVALUATE MODELS WHEN THERE IS A SIGNIFICANT DISTRIBUTION DIFFERENCE BETWEEN TRAIN AND TEST SETS. WE COMPARE OUR PROPOSED METHOD WITH DIFFERENT MULTISPECTRAL PEDESTRIAN DETECTION MODELS [5], [12], [17]–[19], [53], [87] RECENTLY PROPOSED. THE BEST RESULTS ARE HIGHLIGHTED.

VI. EXPERIMENTAL RESULT

A. Result on FLIR, and CVC-14

We train and test on FLIR [31], CVC-14 [32] datasets to evaluate whether our method performs well on general multispectral pedestrian data. We report the detection performance of different models on these datasets. For the evaluation metrics, we use average precision (AP) and log-average miss rate (MR). Following previous works [5], [12], [17]–[19], we report MR performance separately for daytime (‘Day’), nighttime (‘Night’), and the entire set (‘All’), while AP is evaluated on the entire set (‘All’). Note that lower MR (MR \downarrow) and higher AP (AP \uparrow) values indicate better detection performance.

Table I (Left) shows the experimental results on the FLIR and CVC-14 test set. On FLIR, MSCoTDet achieves the highest AP (90.39 AP), and the lowest MR (13.99, 8.38, and 12.16 MR). Such results indicate the effectiveness of MSCoTDet on well-aligned data. On CVC-14, MSCoTDet demonstrates the lowest miss rate among models in (‘Day’), and (‘All’), with a value of 6.69 MR and 10.39 MR, respectively. Also,

the highest AP (92.38 AP) is achieved. As (‘All’) indicates the entire dataset, our method achieves the best performance also on CVC-14. Such results illustrate that MSCoTDet is also effective on a dataset that largely contains misaligned multispectral data.

B. Result on ROTX-MP

Experimenting with models on the ROTX-MP [17] dataset is to evaluate modality bias and their generalizability when there is a significant distributional change in test data. Following the original work [17], we train models on general datasets (FLIR [31], and CVC-14 [32]) and test models on ROTX-MP. The results are in Table I (Right). MSCoTDet achieves the best performance on ROTX-MP for both cases when trained on FLIR and CVC-14. When trained from FLIR, MSCoTDet achieves the highest AP (67.33 AP) and lowest MR (15.23, 24.02, 23.57 MR) which outperforms other methods by at least 10.24 AP, 27.66 MR, 9.17 MR, and 10.06 MR, respectively. When trained from CVC-14, MSCoTDet achieves the highest AP (57.65 AP) and lowest MR (27.16, 34.35, 34.18) which

Train	FLIR				CVC-14				Modality Used		
Test	FLIR				CVC-14						
Metric	AP(↑)	MR(↓)			AP(↑)	MR(↓)					
Method	All	Day	Night	All	All	Day	Night	All	RGB	Thermal	Language
RGB only	76.06	23.23	33.18	26.33	86.54	31.55	40.10	36.07	✓		
Thermal only	85.73	21.56	15.84	20.17	79.72	43.24	33.44	36.07		✓	
Late-fusion	88.60	17.31	11.68	16.14	88.53	18.33	18.86	21.57	✓	✓	
MSCoTDet(Ours)	90.39	13.99	8.38	12.16	92.38	6.69	13.69	10.39	✓	✓	✓

Train	FLIR				CVC-14				Modality Used		
Test	ROTX-MP				ROTX-MP						
Metric	AP(↑)	MR(↓)			AP(↑)	MR(↓)					
Method	All	Day	Night	All	All	Day	Night	All	RGB	Thermal	Language
RGB only	54.20	32.47	36.22	35.61	31.05	30.82	55.39	52.21	✓		
Thermal only	19.33	72.47	67.88	69.04	9.10	91.61	92.41	91.97		✓	
Late-fusion	58.95	27.42	34.89	32.67	44.72	38.82	44.78	42.20	✓	✓	
MSCoTDet(Ours)	67.33	15.23	24.02	23.57	57.65	27.16	34.35	34.18	✓	✓	✓

TABLE II
ABLATION STUDY ON THE EFFECT OF USING LANGUAGE MODELS. OUR FOCUS IS TO COMPARE MSCOTDET WITH ‘LATE-FUSION’, THE VISION BRANCH EQUIPPED WITH VISION-DRIVEN DETECTION OF MSCOTDET.

Train		FLIR				CVC-14			
Test		FLIR				CVC-14			
Metric		AP(↑)	MR(↓)			AP(↑)	MR(↓)		
V	VL	All	Day	Night	All	All	Day	Night	All
Avg	Avg	89.47	15.87	9.94	14.20	89.68	10.98	17.38	16.12
Avg	Max	88.31	16.71	10.76	15.34	88.86	10.26	18.53	15.71
Max	Max	89.94	16.89	9.03	14.57	89.64	8.83	17.54	14.07
Max	Avg	90.39	13.99	8.38	12.16	92.38	6.69	13.69	10.39

Train		FLIR				CVC-14			
Test		ROTX-MP				ROTX-MP			
Metric		AP(↑)	MR(↓)			AP(↑)	MR(↓)		
V	VL	All	Day	Night	All	All	Day	Night	All
Avg	Avg	66.22	20.14	27.20	26.92	56.69	35.56	38.90	36.14
Avg	Max	66.27	28.17	26.89	27.67	56.60	34.80	37.19	36.69
Max	Max	66.31	26.14	25.29	25.78	56.02	31.43	39.38	37.12
Max	Avg	67.33	15.23	24.02	23.57	57.65	27.16	34.35	34.18

TABLE III
ABLATION STUDY ON THE SCORE-FUSION STRATEGY. WE COMPARE THE 1) AVG, AVG, 2) AVG, MAX, 3) MAX, MAX, AND 4) MAX, AVG STRATEGIES IN THE VISION-DRIVEN DETECTION (‘V’) AND IN THE VISION-LANGUAGE FUSION (‘VL’).

outperforms other methods by at least 22.69 AP, 13.41 MR, 10.69 MR, and 8.92 MR, respectively. Such results indicate that MSCoTDet has a better ability to intervene in modality bias compared to other models.

C. Comparison with Competing Methods that Provided Access to an LLM

For a fair comparison, we also evaluate the competing methods [5], [12], [17]–[19], [53], [87] that provided access to using a pre-trained LLM [35], [38]. As with MSCoTDet, text descriptions of RGB/thermal pedestrians are generated with an MLLM [35]. The same MSCoTDet implementations are adopted for competing methods of late-fusion [19]. For competing methods of mid-fusion [5], [12], [17], [18], [53], [87], we modify MSCoT prompting and LMF to ensure compatibility. The modifications involved using the same bounding box regions for RGB and thermal images in MSCoT Prompting, (i.e., $B_{RGB}^V = B_T^V = B_F^V$ in Eq.11) since mid-fusion models produce only fused outputs. Accordingly, the LMF is modified to substitute B_F^V to B_F^L in Eq.12. Other processes are kept the same, and the evaluation is performed with the detection results obtained through Eq.12.

The results of the Halfway Fusion [5] + LLM, CFT [18]+LLM, Kim et al. [12] + LLM, CMM [17] + LLM, ProbEn [19] + LLM, ICAFusion [87] + LLM, MS-DETR [53] + LLM on the FLIR [31] dataset, CVC-14 [32], and ROTX-MP [17] are shown in TABLE I. MSCoTDet consistently outperforms these competing methods on all datasets as other methods show only marginal improvements or even degrade with LLM integration. These results suggest that MSCoTDet effectively incorporates the LLM into the detection process, and thereby enhances detection accuracy.

VII. ABLATION STUDY

A. Effect of Integrating Language Models

We conduct an ablation study to evaluate the effectiveness of integrating large language models to our framework. As our framework fuses detection results from both the vision branch and the language branch, one might ask: *how much does the language branch boost overall performance?* For the ablation study, we compare MSCoTDet and three detection models: (1) ‘RGB only’, (2) ‘Thermal only’, and (3) ‘Late-fusion’. First, the ‘RGB only’, and the ‘Thermal only’ model indicate single-modal detection in the vision branch of MSCoTDet. Second, ‘Late-fusion’ is in which the single-modal detections of ‘RGB only’ and ‘Thermal only’ are fused, i.e., equivalent to the vision branch equipped with vision-driven detection of our framework. Thus, to measure the effect of using large language models, our main focus is to compare ‘Late-fusion’ with MSCoTDet. The results are shown in Table II. Our method achieves higher performance than ‘Late-fusion’ in all FLIR [31], CVC-14 [32], and ROTX-MP [17]. The results on the FLIR and CVC-14 indicate that integrating large language models can improve the overall performance of multispectral pedestrian detectors in general datasets. Also, the results on ROTX-MP indicate that using language models can significantly improve the generalizability of multispectral pedestrian detectors, and effectively mitigate the modality bias.

B. Effect of the Fusion Strategy

We conduct an ablation study to evaluate the design choice of our fusion strategy in Section IV-D. Our fusion strategies include score-fusion and box-fusion. For score-fusion, we adopt the Non-maximum Suppression (NMS) in the vision-driven detection (‘V’) and averaging strategy in the vision-language fusion (‘VL’), respectively. NMS compares the prediction scores estimated in each modality and votes for the highest

Train			FLIR						CVC-14					
Test			FLIR						CVC-14					
Method			AP(\uparrow)		MR(\downarrow)				AP(\uparrow)		MR(\downarrow)			
V	L	VL	All	Day	Night	All	All	Day	Night	All	All	Day	Night	All
argmax	argmax	argmax	89.49	15.31	9.43	13.65	91.06	7.56	17.64	14.00	argmax	argmax	argmax	66.10
s-avg	argmax	argmax	89.79	14.59	8.82	12.75	91.60	8.03	15.28	12.63	s-avg	argmax	argmax	66.29
argmax	s-avg	argmax	89.83	14.88	8.97	13.12	90.86	8.32	15.39	13.31	argmax	s-avg	argmax	67.03
s-avg	s-avg	argmax	90.32	14.22	8.77	12.47	91.72	7.60	15.14	12.54	s-avg	s-avg	argmax	67.24
argmax	argmax	s-avg	89.49	15.07	8.73	13.18	90.71	6.25	18.51	14.18	argmax	argmax	s-avg	66.11
s-avg	argmax	s-avg	90.32	14.25	8.55	12.43	92.12	7.63	15.19	11.99	s-avg	argmax	s-avg	67.28
argmax	s-avg	s-avg	89.73	14.13	9.26	12.76	91.41	6.85	16.81	13.47	argmax	s-avg	s-avg	67.15
s-avg	s-avg	s-avg	90.39	13.99	8.38	12.16	92.38	6.69	13.69	10.39	s-avg	s-avg	s-avg	67.33

TABLE IV

ABLATION STUDY ON THE BOX-FUSION STRATEGY. WE EXPERIMENT ARGMAX AND S-AVG FOR EACH VISION-DRIVEN DETECTION ('V'), LANGUAGE-DRIVEN DETECTION ('L'), AND VISION-LANGUAGE FUSION ('VL').

Train			FLIR						CVC-14					
Test			FLIR						CVC-14					
Metric			AP(\uparrow)		MR(\downarrow)				AP(\uparrow)		MR(\downarrow)			
Metric			All	Day	Night	All	All	Day	Night	All	All	Day	Night	All
Phantom-7B [94]			90.08	16.31	8.88	13.84	91.51	8.46	14.19	11.32	Phantom-7B [94]			66.22
InternVL-8B [95]			90.18	15.73	9.18	13.78	91.48	8.56	14.75	11.29	InternVL-8B [95]			66.32
Gemini-1.5 Pro [96]			90.31	16.29	7.62	13.53	92.02	9.51	14.51	11.46	Gemini-1.5 Pro [96]			66.94
GPT-4V [35]			90.39	13.99	8.38	12.16	92.38	6.69	13.69	10.39	GPT-4V [35]			67.33

TABLE V

ABLATION STUDY OF USING DIFFERENT MLLM MODELS FOR GENERATING TEXT DESCRIPTIONS. FOUR DIFFERENT MODELS (PHANTOM-7B [94], INTERNVL-8B [95], GEMINI-1.5 PRO [96], GPT-4V [35]) ARE USED FOR THE EXPERIMENTS. EXPERIMENTS ARE CONDUCTED ON FLIR, CVC-14 AND ROTX-MP DATASETS.

one, removing the lower scores (Eq. 2). The averaging strategy averages prediction scores estimated in each modality (Eq. 1). Denote the averaging strategy as 'Avg' and NMS as 'Max'. For the comparison study, we conducted experiments on the (1) Avg, Avg, (2) Avg, Max, and (3) Max, Max fusion strategies in each vision-driven detection ('V') and vision-language fusion ('VL'), respectively. We do not compare different score-fusion in the language branch, as we use our proposed method: MSCoT (Section IV-C) produces prediction scores from fused modalities. All other conditions are kept the same. The results are shown in Table III. The Max, Avg strategy consistently performs the best in all test sets.

For box-fusion, we adopt weighted averaging (Eq. 3) for all vision-driven detection ('V'), language-driven detection ('L'), and vision-language fusion ('VL'). Denote the weighted averaging strategy as 's-avg'. For the comparison study, we consider the NMS box fusion, denoted as 'argmax', and compare between a total of 8 combinations (either s-avg or max in three parts). All other conditions are kept the same as our MSCoTDet design during all experiments. The results are shown in Table IV. Applying s-avg for all V, L, and VL shows the best performance for most test cases.

C. Impact of Using Different MLLM Models for Generating Text Descriptions

We conduct an ablation study to evaluate the impact of using different MLLM models for generating text descriptions. MSCoTDet is tested with four different MLLMs: Phantom-7B [94], InternVL-8B [95], Gemini-1.5 Pro [96] and GPT-4V [35]. Throughout these experiments, other components of

Method	Running Time (s)	Use of the Language Model
MSCoTDet without language branch	0.16	
MSCoTDet	0.20	✓

TABLE VI

COMPUTATIONAL COMPARISON ON THE MODEL EFFICIENCY REGARDING THE INCLUSION OF THE LANGUAGE MODEL. THE AVERAGE RUNNING TIME (SECONDS PER IMAGE) OF MSCoTDet WITH AND WITHOUT THE LANGUAGE BRANCH IS EVALUATED ON THE FLIR [31] DATASET.

MSCoTDet remained the same.

The results in Table V show that MSCoTDet maintains consistent performance across the various MLLMs used for text generation, with the best results obtained with GPT-4V. This indicates that MSCoTDet remains robust regardless of the specific MLLM used, making it adaptable and effective across different MLLMs.

D. Impact of the Inclusion of the Language Model on the Model's Efficiency

To quantitatively analyze how the inclusion of the language model affects the model's efficiency, we compare MSCoTDet with and without the language branch. The MSCoTDet without the language branch is equivalent to the visual branch of the MSCoTDet alone. The computational comparison was conducted by measuring the model's average running time (seconds per image) on the FLIR [31] dataset, using a single Nvidia A6000 GPU. The results reported in Table VI show that the running time of MSCoTDet with and without the language branch is 0.20 seconds and 0.16 seconds per image, respectively. Thus, the inclusion of the language model adds an additional 0.04 seconds per image to the running time.

VIII. DISCUSSION

Limitation and Future Work. The goal of our work is to address modality bias in multispectral pedestrian detection and enhance detection accuracy using large language models (LLMs). A limitation is that our work focuses on a single class: pedestrians. As language models can generate descriptions and detection scores for classes other than pedestrians, our Multispectral Chain-of-Thought (MSCoT) prompting method can potentially be integrated into object detection on general target classes. Moreover, Language-Driven Multi-modal Fusion (LMF) is applicable to fuse the detection results of various classes by conducting class-wise operations in eq.10-eq.12. We plan to extend our work to other object classes in future work.

Applicability to Other Multi-modality Tasks. Our proposed methods can be potentially applied in other multi-modality fusion tasks in computer vision. For instance, our strategies of integrating textual descriptions across different modalities can help to train models when there are insufficient annotations, e.g., as in scribble-supervised RGB-D saliency detection [97]. Another potential application is in the medical field, where multiple imaging modalities (e.g., T1-weighted, T1-contrast, T2-weighted, and FLAIR MRIs) are used in combination to detect/segment lesions (e.g., brain tumor segmentation [98], [99]). Our technique of generating detection rationales from multi-modal images can be applied to generate clinical evidence when detecting lesions from multiple medical images.

IX. CONCLUSION

In this paper, we introduced MSCoTDet, a novel framework for enhancing multispectral pedestrian detection by addressing modality bias using a Large Language Model (LLM). The framework employs a Multispectral Chain-of-Thought (MSCoT) prompting strategy to guide an LLM in performing multispectral detection tasks, integrating this with vision-based models through a Language-driven Multi-modal Fusion (LMF) approach. Our extensive experiments demonstrated that MSCoTDet outperforms existing methods on standard datasets such as FLIR and CVC-14, achieving significant improvements in Average Precision (AP) and Miss Rates. Furthermore, MSCoTDet achieved impressive performance on the ROTX-MP dataset, proving the generalizability, particularly in scenarios with distribution shifts between training and testing data.

REFERENCES

- [1] Yiming Sun, Bing Cao, Pengfei Zhu, and Qinghua Hu, "Drone-based rgb-infrared cross-modality vehicle detection via uncertainty-aware learning," *IEEE Transactions on Circuits and Systems for Video Technology*, vol. 32, no. 10, pp. 6700–6713, 2022.
- [2] Dayan Guan, Yanpeng Cao, Jiangxin Yang, Yanlong Cao, and Michael Ying Yang, "Fusion of multispectral data through illumination-aware deep neural networks for pedestrian detection," *Information Fusion*, vol. 50, pp. 148–157, 2019.
- [3] Taeheon Kim, Youngjoon Yu, and Yong Man Ro, "Multispectral invisible coating: laminated visible-thermal physical attack against multispectral object detectors using transparent low-e films," in *Proceedings of the AAAI Conference on Artificial Intelligence*, 2023, vol. 37, pp. 1151–1159.
- [4] Dan Xu, Wanli Ouyang, Elisa Ricci, Xiaogang Wang, and Nicu Sebe, "Learning cross-modal deep representations for robust pedestrian detection," in *Proceedings of the IEEE conference on computer vision and pattern recognition*, 2017, pp. 5363–5371.
- [5] Jingjing Liu, Shaoting Zhang, Shu Wang, and Dimitris N Metaxas, "Multispectral deep neural networks for pedestrian detection," *arXiv preprint arXiv:1611.02644*, 2016.
- [6] Chengyang Li, Dan Song, Ruofeng Tong, and Min Tang, "Illumination-aware faster r-cnn for robust multispectral pedestrian detection," *Pattern Recognition*, vol. 85, pp. 161–171, 2019.
- [7] Lu Zhang, Zhiyong Liu, Shifeng Zhang, Xu Yang, Hong Qiao, Kaizhu Huang, and Amir Hussain, "Cross-modality interactive attention network for multispectral pedestrian detection," *Information Fusion*, vol. 50, pp. 20–29, 2019.
- [8] Lu Zhang, Xiangyu Zhu, Xiangyu Chen, Xu Yang, Zhen Lei, and Zhiyong Liu, "Weakly aligned cross-modal learning for multispectral pedestrian detection," in *Proceedings of the IEEE/CVF international conference on computer vision*, 2019, pp. 5127–5137.
- [9] Taeheon Kim, Hong Joo Lee, and Yong Man Ro, "Map: Multispectral adversarial patch to attack person detection," in *ICASSP 2022-2022 IEEE International Conference on Acoustics, Speech and Signal Processing (ICASSP)*. IEEE, 2022, pp. 4853–4857.
- [10] Taeheon Kim, Sangyun Chung, Youngjoon Yu, and Yong Man Ro, "Revisiting misalignment in multispectral pedestrian detection: a language-driven approach for cross-modal alignment fusion," in *2024 IEEE International Conference on Image Processing Challenges and Workshops (ICIPCW)*. IEEE, 2024, pp. 4217–4222.
- [11] Taeheon Kim, Sebin Shin, Youngjoon Yu, Hak Gu Kim, and Yong Man Ro, "Mitigating uni-modal sensory bias in multimodal object detection with counterfactual intervention and causal mode multiplexing," 2024.
- [12] Jung Uk Kim, Sungjune Park, and Yong Man Ro, "Uncertainty-guided cross-modal learning for robust multispectral pedestrian detection," *IEEE Transactions on Circuits and Systems for Video Technology*, vol. 32, no. 3, pp. 1510–1523, 2021.
- [13] Soonmin Hwang, Jaesik Park, Namil Kim, Yookyung Choi, and In So Kweon, "Multispectral pedestrian detection: Benchmark dataset and baseline," in *Proceedings of the IEEE conference on computer vision and pattern recognition*, 2015, pp. 1037–1045.
- [14] Kailai Zhou, Linsen Chen, and Xun Cao, "Improving multispectral pedestrian detection by addressing modality imbalance problems," in *Computer Vision–ECCV 2020: 16th European Conference, Glasgow, UK, August 23–28, 2020, Proceedings, Part XVIII 16*. Springer, 2020, pp. 787–803.
- [15] Qing Li, Changqing Zhang, Qinghua Hu, Pengfei Zhu, Huazhu Fu, and Lei Chen, "Stabilizing multispectral pedestrian detection with evidential hybrid fusion," *IEEE Transactions on Circuits and Systems for Video Technology*, 2023.
- [16] Jörg Wagner, Volker Fischer, Michael Herman, Sven Behnke, et al., "Multispectral pedestrian detection using deep fusion convolutional neural networks," in *ESANN*, 2016, vol. 587, pp. 509–514.
- [17] Taeheon Kim, Sebin Shin, Youngjoon Yu, Hak Gu Kim, and Yong Man Ro, "Causal mode multiplexer: A novel framework for unbiased multispectral pedestrian detection," in *Proceedings of the IEEE/CVF Conference on Computer Vision and Pattern Recognition (CVPR)*, June 2024, pp. 26784–26793.
- [18] Fang Qingyun, Han Dapeng, and Wang Zhaokui, "Cross-modality fusion transformer for multispectral object detection," 2022.
- [19] Yi-Ting Chen, Jinghao Shi, Zelin Ye, Christoph Mertz, Deva Ramanan, and Shu Kong, "Multimodal object detection via probabilistic ensembling," in *European Conference on Computer Vision*. Springer, 2022, pp. 139–158.
- [20] Taeheon Kim, Youngjoon Yu, and Yong Man Ro, "Defending physical adversarial attack on object detection via adversarial patch-feature energy," in *Proceedings of the 30th ACM International Conference on Multimedia*, 2022, pp. 1905–1913.
- [21] Piotr Dollar, Christian Wojek, Bernt Schiele, and Pietro Perona, "Pedestrian detection: An evaluation of the state of the art," *IEEE transactions on pattern analysis and machine intelligence*, vol. 34, no. 4, pp. 743–761, 2011.
- [22] Wei-Yen Hsu and Wen-Yen Lin, "Ratio-and-scale-aware yolo for pedestrian detection," *IEEE transactions on image processing*, vol. 30, pp. 934–947, 2020.
- [23] Irtiza Hasan, Shengcai Liao, Jinpeng Li, Saad Ullah Akram, and Ling Shao, "Generalizable pedestrian detection: The elephant in the room," in *Proceedings of the IEEE/CVF Conference on Computer Vision and Pattern Recognition*, 2021, pp. 11328–11337.
- [24] Xinwen Fan, Yukang Zhang, Yang Lu, and Hanzi Wang, "Parformer: transformer-based multi-task network for pedestrian attribute recognition," *IEEE Transactions on Circuits and Systems for Video Technology*, 2023.
- [25] Sungjune Park, Hyunjun Kim, and Yong Man Ro, "Integrating language-derived appearance elements with visual cues in pedestrian detection," *IEEE Transactions on Circuits and Systems for Video Technology*, 2024.

- [26] Yi Shi, Shixuan Zhao, Jiang Wu, Zhangbi Wu, and Hongmei Yan, "Fixated object detection based on saliency prior in traffic scenes," *IEEE Transactions on Circuits and Systems for Video Technology*, 2023.
- [27] Muhammad Bilal, Asim Khan, Muhammad Umar Karim Khan, and Chong-Min Kyung, "A low-complexity pedestrian detection framework for smart video surveillance systems," *IEEE Transactions on Circuits and Systems for Video Technology*, vol. 27, no. 10, pp. 2260–2273, 2016.
- [28] Mira Jeong, Byoung Chul Ko, and Jae-Yeal Nam, "Early detection of sudden pedestrian crossing for safe driving during summer nights," *IEEE transactions on circuits and systems for video technology*, vol. 27, no. 6, pp. 1368–1380, 2016.
- [29] Xiaoyu Chen, Hongliang Li, Qingbo Wu, King Ngi Ngan, and Linfeng Xu, "High-quality r-cnn object detection using multi-path detection calibration network," *IEEE Transactions on Circuits and Systems for Video Technology*, vol. 31, no. 2, pp. 715–727, 2020.
- [30] Jung Uk Kim, Jongsu Kwon, Hak Gu Kim, and Yong Man Ro, "Bbc net: Bounding-box critic network for occlusion-robust object detection," *IEEE transactions on circuits and systems for video technology*, vol. 30, no. 4, pp. 1037–1050, 2019.
- [31] Inc FLIR Systems, "Free teledyne flir thermal dataset for algorithm training," <https://www.flir.com/oem/adas/adas-dataset-form/>, 2021, Accessed: 2022-08-05.
- [32] Alejandro González, Zhijie Fang, Yainuvis Socarras, Joan Serrat, David Vázquez, Jiaolong Xu, and Antonio M López, "Pedestrian detection at day/night time with visible and fir cameras: A comparison," *Sensors*, vol. 16, no. 6, pp. 820, 2016.
- [33] Yulei Niu, Kaihua Tang, Hanwang Zhang, Zhiwu Lu, Xian-Sheng Hua, and Ji-Rong Wen, "Counterfactual vqa: A cause-effect look at language bias," in *Proceedings of the IEEE/CVF Conference on Computer Vision and Pattern Recognition*, 2021, pp. 12700–12710.
- [34] Enkelejda Kasneci, Kathrin Seblner, Stefan Küchemann, Maria Bannert, Daryna Dementieva, Frank Fischer, Urs Gasser, Georg Groh, Stephan Günnemann, Eyke Hüllermeier, et al., "Chatgpt for good? on opportunities and challenges of large language models for education," *Learning and individual differences*, vol. 103, pp. 102274, 2023.
- [35] Josh Achiam, Steven Adler, Sandhini Agarwal, Lama Ahmad, Ilge Akkaya, Florencia Leoni Aleman, Diogo Almeida, Janko Altschmidt, Sam Altman, Shyamal Anadkat, et al., "Gpt-4 technical report," *arXiv preprint arXiv:2303.08774*, 2023.
- [36] Haotian Liu, Chunyuan Li, Qingyang Wu, and Yong Jae Lee, "Visual instruction tuning," *Advances in neural information processing systems*, vol. 36, 2024.
- [37] Jason Wei, Zuehzi Wang, Dale Schuurmans, Maarten Bosma, Fei Xia, Ed Chi, Quoc V Le, Denny Zhou, et al., "Chain-of-thought prompting elicits reasoning in large language models," *Advances in Neural Information Processing Systems*, vol. 35, pp. 24824–24837, 2022.
- [38] Inc OpenAI, "Chatgpt-3.5 turbo api," <https://chat.openai.com/>, 2023, Accessed: 2024-02-29.
- [39] Miao Xiong, Zhiyuan Hu, Xinyang Lu, Yifei Li, Jie Fu, Junxian He, and Bryan Hooi, "Can llms express their uncertainty? an empirical evaluation of confidence elicitation in llms," *arXiv preprint arXiv:2306.13063*, 2023.
- [40] Moxin Li, Wenjie Wang, Fuli Feng, Fengbin Zhu, Qifan Wang, and Tat-Seng Chua, "Think twice before assure: Confidence estimation for large language models through reflection on multiple answers," *arXiv preprint arXiv:2403.09972*, 2024.
- [41] Gianluca Detommaso, Martin Bertran, Riccardo Fogliato, and Aaron Roth, "Multicalibration for confidence scoring in llms," *arXiv preprint arXiv:2404.04689*, 2024.
- [42] Gwenth Portillo Wightman, Alexandra DeLucia, and Mark Dredze, "Strength in numbers: Estimating confidence of large language models by prompt agreement," in *Proceedings of the 3rd Workshop on Trustworthy Natural Language Processing (TrustNLP 2023)*, 2023, pp. 326–362.
- [43] Nan Pu, Wei Chen, Yu Liu, Erwin M Bakker, and Michael S Lew, "Dual gaussian-based variational subspace disentanglement for visible-infrared person re-identification," in *Proceedings of the 28th ACM international conference on multimedia*, 2020, pp. 2149–2158.
- [44] Chuchu Han, Jiacheng Ye, Yunshan Zhong, Xin Tan, Chi Zhang, Changxin Gao, and Nong Sang, "Re-id driven localization refinement for person search," in *Proceedings of the IEEE/CVF International Conference on Computer Vision*, 2019, pp. 9814–9823.
- [45] Jiale Cao, Yanwei Pang, Shengjie Zhao, and Xuelong Li, "High-level semantic networks for multi-scale object detection," *IEEE Transactions on Circuits and Systems for Video Technology*, vol. 30, no. 10, pp. 3372–3386, 2019.
- [46] Jung Uk Kim, Seong Tae Kim, Hong Joo Lee, Sangmin Lee, and Yong Man Ro, "Cua loss: Class uncertainty-aware gradient modulation for robust object detection," *IEEE Transactions on Circuits and Systems for Video Technology*, vol. 31, no. 9, pp. 3529–3543, 2020.
- [47] Shifeng Zhang, Longyin Wen, Zhen Lei, and Stan Z Li, "Refinedet++: Single-shot refinement neural network for object detection," *IEEE Transactions on Circuits and Systems for Video Technology*, vol. 31, no. 2, pp. 674–687, 2020.
- [48] Wanli Ouyang, Xingyu Zeng, and Xiaogang Wang, "Partial occlusion handling in pedestrian detection with a deep model," *IEEE Transactions on Circuits and Systems for Video Technology*, vol. 26, no. 11, pp. 2123–2137, 2015.
- [49] Yifan Jiao, Hantao Yao, and Changsheng Xu, "Pen: Pose-embedding network for pedestrian detection," *IEEE Transactions on Circuits and Systems for Video Technology*, vol. 31, no. 3, pp. 1150–1162, 2020.
- [50] Sungjune Park, Hyunjun Kim, and Yong Man Ro, "Robust pedestrian detection via constructing versatile pedestrian knowledge bank," *Pattern Recognition*, p. 110539, 2024.
- [51] Youngjoon Yu, Hong Joo Lee, Hakmin Lee, and Yong Man Ro, "Defending person detection against adversarial patch attack by using universal defensive frame," *IEEE Transactions on Image Processing*, vol. 31, pp. 6976–6990, 2022.
- [52] Chengyang Li, Dan Song, Ruofeng Tong, and Min Tang, "Multispectral pedestrian detection via simultaneous detection and segmentation," *arXiv preprint arXiv:1808.04818*, 2018.
- [53] Yinghui Xing, Shuo Yang, Song Wang, Shizhou Zhang, Guoqiang Liang, Xiuwei Zhang, and Yanning Zhang, "Ms-detr: Multispectral pedestrian detection transformer with loosely coupled fusion and modality-balanced optimization," *IEEE Transactions on Intelligent Transportation Systems*, 2024.
- [54] Xizhou Zhu, Weijie Su, Lewei Lu, Bin Li, Xiaogang Wang, and Jifeng Dai, "Deformable detr: Deformable transformers for end-to-end object detection," *arXiv preprint arXiv:2010.04159*, 2020.
- [55] Weiyao Wang, Du Tran, and Matt Feiszli, "What makes training multi-modal classification networks hard?," in *Proceedings of the IEEE/CVF conference on computer vision and pattern recognition*, 2020, pp. 12695–12705.
- [56] Xulin Li, Yan Lu, Bin Liu, Yating Liu, Guojun Yin, Qi Chu, Jinyang Huang, Feng Zhu, Rui Zhao, and Nenghai Yu, "Counterfactual intervention feature transfer for visible-infrared person re-identification," in *European conference on computer vision*. Springer, 2022, pp. 381–398.
- [57] Ehsan Abbasnejad, Damien Teney, Amin Parvaneh, Javen Shi, and Anton van den Hengel, "Counterfactual vision and language learning," in *Proceedings of the IEEE/CVF conference on computer vision and pattern recognition*, 2020, pp. 10044–10054.
- [58] Zujie Liang, Weitao Jiang, Haifeng Hu, and Jiaying Zhu, "Learning to contrast the counterfactual samples for robust visual question answering," in *Proceedings of the 2020 conference on empirical methods in natural language processing (EMNLP)*, 2020, pp. 3285–3292.
- [59] Tejas Gokhale, Pratyay Banerjee, Chitta Baral, and Yezhou Yang, "Mutant: A training paradigm for out-of-distribution generalization in visual question answering," *arXiv preprint arXiv:2009.08566*, 2020.
- [60] Long Chen, Xin Yan, Jun Xiao, Hanwang Zhang, Shiliang Pu, and Yuetong Zhuang, "Counterfactual samples synthesizing for robust visual question answering," in *Proceedings of the IEEE/CVF conference on computer vision and pattern recognition*, 2020, pp. 10800–10809.
- [61] Aishwarya Agrawal, Dhruv Batra, Devi Parikh, and Aniruddha Kembhavi, "Don't just assume; look and answer: Overcoming priors for visual question answering," in *Proceedings of the IEEE conference on computer vision and pattern recognition*, 2018, pp. 4971–4980.
- [62] Itai Gat, Idan Schwartz, Alexander Schwing, and Tamir Hazan, "Removing bias in multi-modal classifiers: Regularization by maximizing functional entropies," *Advances in Neural Information Processing Systems*, vol. 33, pp. 3197–3208, 2020.
- [63] Long Ouyang, Jeffrey Wu, Xu Jiang, Diogo Almeida, Carroll Wainwright, Pamela Mishkin, Chong Zhang, Sandhini Agarwal, Katarina Slama, Alex Ray, et al., "Training language models to follow instructions with human feedback," *Advances in Neural Information Processing Systems*, vol. 35, pp. 27730–27744, 2022.
- [64] Tom Brown, Benjamin Mann, Nick Ryder, Melanie Subbiah, Jared D Kaplan, Prafulla Dhariwal, Arvind Neelakantan, Pranav Shyam, Girish Sastry, Amanda Askell, et al., "Language models are few-shot learners," *Advances in neural information processing systems*, vol. 33, pp. 1877–1901, 2020.
- [65] BigScience Workshop, Teven Le Scao, Angela Fan, Christopher Akiki, Ellie Pavlick, Suzana Ilić, Daniel Hesslow, Roman Castagné, Alexandra Sasha Luccioni, François Yvon, et al., "Bloom: A 176b-parameter open-access multilingual language model," *arXiv preprint arXiv:2211.05100*, 2022.
- [66] Hugo Touvron, Thibaut Lavril, Gautier Izacard, Xavier Martinet, Marie-Anne Lachaux, Timothée Lacroix, Baptiste Rozière, Naman Goyal, Eric Hambro, Faisal Azhar, et al., "Llama: Open and efficient foundation language models," *arXiv preprint arXiv:2302.13971*, 2023.
- [67] Aakanksha Chowdhery, Sharan Narang, Jacob Devlin, Maarten Bosma, Gaurav Mishra, Adam Roberts, Paul Barham, Hyung Won Chung, Charles Sutton, Sebastian Gehrmann, et al., "Palm: Scaling language modeling with pathways," *Journal of Machine Learning Research*, vol. 24, no. 240, pp. 1–113, 2023.
- [68] Jordan Hoffmann, Sebastian Borgeaud, Arthur Mensch, Elena Buchatskaya, Trevor Cai, Eliza Rutherford, Diego de Las Casas, Lisa Anne Hendricks, Johannes Welbl, Aidan Clark, et al., "Training compute-optimal large language models," *arXiv preprint arXiv:2203.15556*, 2022.

- [69] Yue Yang, Artemis Panagopoulou, Shenghao Zhou, Daniel Jin, Chris Callison-Burch, and Mark Yatskar, "Language in a bottle: Language model guided concept bottlenecks for interpretable image classification," in *Proceedings of the IEEE/CVF Conference on Computer Vision and Pattern Recognition*, 2023, pp. 19187–19197.
- [70] Muhammad Ferjad Naeem, Muhammad Gul Zain Ali Khan, Yongqin Xian, Muhammad Zeshan Afzal, Didier Stricker, Luc Van Gool, and Federico Tombari, "I2mvformer: Large language model generated multi-view document supervision for zero-shot image classification," in *Proceedings of the IEEE/CVF Conference on Computer Vision and Pattern Recognition*, 2023, pp. 15169–15179.
- [71] Zaid Khan, Vijay Kumar BG, Samuel Schuster, Xiang Yu, Yun Fu, and Manmohan Chandraker, "Q: How to specialize large vision-language models to data-scarce vqa tasks? a: Self-train on unlabeled images!," in *Proceedings of the IEEE/CVF Conference on Computer Vision and Pattern Recognition*, 2023, pp. 15005–15015.
- [72] Cees GM Snoek, Marcel Worring, and Arnold WM Smeulders, "Early versus late fusion in semantic video analysis," in *Proceedings of the 13th annual ACM international conference on Multimedia*, 2005, pp. 399–402.
- [73] Georgios Tzifas and Hamidreza Kasaei, "Early or late fusion matters: Efficient rgb-d fusion in vision transformers for 3d object recognition," in *2023 IEEE/RSJ International Conference on Intelligent Robots and Systems (IROS)*. IEEE, 2023, pp. 9558–9565.
- [74] Tri Minh Nguyen, Thin Nguyen, Thao Minh Le, and Truyen Tran, "Gefa: early fusion approach in drug-target affinity prediction," *IEEE/ACM transactions on computational biology and bioinformatics*, vol. 19, no. 2, pp. 718–728, 2021.
- [75] Chen Chen, Ruizhe Li, Yuchen Hu, Sabato Marco Siniscalchi, Pin-Yu Chen, Ensiong Chng, and Chao-Han Huck Yang, "It's never too late: Fusing acoustic information into large language models for automatic speech recognition," *arXiv preprint arXiv:2402.05457*, 2024.
- [76] Emilie Morvant, Amaury Habrard, and Stéphane Ayache, "Majority vote of diverse classifiers for late fusion," in *Structural, Syntactic, and Statistical Pattern Recognition: Joint IAPR International Workshop, S+ SSPR 2014, Joensuu, Finland, August 20-22, 2014. Proceedings*. Springer, 2014, pp. 153–162.
- [77] Ekaterina Shutova, Douwe Kiela, and Jean Maillard, "Black holes and white rabbits: Metaphor identification with visual features," in *Proceedings of the 2016 conference of the North American chapter of the association for computational linguistics: Human language technologies*, 2016, pp. 160–170.
- [78] Yiqun Yao and Rada Mihalcea, "Modality-specific learning rates for effective multimodal additive late-fusion," in *Findings of the Association for Computational Linguistics: ACL 2022*, 2022, pp. 1824–1834.
- [79] Jack Hessel and Lillian Lee, "Does my multimodal model learn cross-modal interactions? it's harder to tell than you might think!," *arXiv preprint arXiv:2010.06572*, 2020.
- [80] Yagya Raj Pandeya and Joonwhoan Lee, "Deep learning-based late fusion of multimodal information for emotion classification of music video," *Multimedia Tools and Applications*, vol. 80, pp. 2887–2905, 2021.
- [81] Jiarui Zhang, Mahyar Khayatkhoei, Prateek Chhikara, and Filip Ilievski, "Visual cropping improves zero-shot question answering of multimodal large language models," *arXiv preprint arXiv:2310.16033*, 2023.
- [82] Inc OpenAI, "Gpt-3.5 turbo fine-tuning and api updates," <https://openai.com/blog/gpt-3-5-turbo-fine-tuning-and-api-updates>, 2023, Accessed: 2024-02-29.
- [83] Heng Zhang, Elisa Fromont, Sébastien Lefevre, and Bruno Avignon, "Multispectral fusion for object detection with cyclic fuse-and-refine blocks," in *2020 IEEE International conference on image processing (ICIP)*. IEEE, 2020, pp. 276–280.
- [84] Zhuofan Zong, Guanglu Song, and Yu Liu, "Detrs with collaborative hybrid assignments training," in *Proceedings of the IEEE/CVF international conference on computer vision*, 2023, pp. 6748–6758.
- [85] Nicolas Carion, Francisco Massa, Gabriel Synnaeve, Nicolas Usunier, Alexander Kirillov, and Sergey Zagoruyko, "End-to-end object detection with transformers," 2020.
- [86] Ilya Loshchilov and Frank Hutter, "Decoupled weight decay regularization," *arXiv preprint arXiv:1711.05101*, 2017.
- [87] Jifeng Shen, Yifei Chen, Yue Liu, Xin Zuo, Heng Fan, and Wankou Yang, "Icafusion: Iterative cross-attention guided feature fusion for multispectral object detection," *Pattern Recognition*, vol. 145, pp. 109913, 2024.
- [88] Ross Girshick, "Fast r-cnn," in *Proceedings of the IEEE international conference on computer vision*, 2015, pp. 1440–1448.
- [89] Shun-ichi Amari, "Backpropagation and stochastic gradient descent method," *Neurocomputing*, vol. 5, no. 4-5, pp. 185–196, 1993.
- [90] Tsung-Yi Lin, Michael Maire, Serge Belongie, James Hays, Pietro Perona, Deva Ramanan, Piotr Dollár, and C Lawrence Zitnick, "Microsoft coco: Common objects in context," in *Computer Vision—ECCV 2014: 13th European Conference, Zurich, Switzerland, September 6-12, 2014, Proceedings, Part V 13*. Springer, 2014, pp. 740–755.
- [91] Yuxin Wu, Alexander Kirillov, Francisco Massa, Wan-Yen Lo, and Ross Girshick, "Detectron2," <https://github.com/facebookresearch/detectron2>, 2019.
- [92] Kaiping He, Xiangyu Zhang, Shaoqing Ren, and Jian Sun, "Deep residual learning for image recognition," in *Proceedings of the IEEE conference on computer vision and pattern recognition*, 2016, pp. 770–778.
- [93] Diederik P Kingma, "Adam: A method for stochastic optimization," *arXiv preprint arXiv:1412.6980*, 2014.
- [94] Byung-Kwan Lee, Sangyun Chung, Chae Won Kim, Beomchan Park, and Yong Man Ro, "Phantom of latent for large language and vision models," *arXiv preprint arXiv:2409.14713*, 2024.
- [95] Zhe Chen, Jiannan Wu, Wenhai Wang, Weijie Su, Guo Chen, Sen Xing, Muyan Zhong, Qinglong Zhang, Xizhou Zhu, Lewei Lu, et al., "Internvl: Scaling up vision foundation models and aligning for generic visual-linguistic tasks," in *Proceedings of the IEEE/CVF Conference on Computer Vision and Pattern Recognition*, 2024, pp. 24185–24198.
- [96] Gemini Team, Rohan Anil, Sebastian Borgeaud, Yonghui Wu, Jean-Baptiste Alayrac, Jiahui Yu, Radu Soricut, Johan Schalkwyk, Andrew M Dai, Anja Hauth, et al., "Gemini: a family of highly capable multimodal models," *arXiv preprint arXiv:2312.11805*, 2023.
- [97] Long Li, Junwei Han, Nian Liu, Salman Khan, Hisham Cholakkal, Rao Muhammad Anwer, and Fahad Shahbaz Khan, "Robust perception and precise segmentation for scribble-supervised rgb-d saliency detection," *IEEE Transactions on Pattern Analysis and Machine Intelligence*, 2023.
- [98] Dingwen Zhang, Guohai Huang, Qiang Zhang, Jungong Han, Junwei Han, and Yizhou Yu, "Cross-modality deep feature learning for brain tumor segmentation," *Pattern Recognition*, vol. 110, pp. 107562, 2021.
- [99] Dingwen Zhang, Guohai Huang, Qiang Zhang, Jungong Han, Junwei Han, Yizhou Wang, and Yizhou Yu, "Exploring task structure for brain tumor segmentation from multi-modality mr images," *IEEE Transactions on Image Processing*, vol. 29, pp. 9032–9043, 2020.



TAEHEON KIM received the B.S. degree in electrical engineering from Korea Advanced Institute of Science and Technology (KAIST), Daejeon, South Korea in 2019. He is currently pursuing the Ph.D. in electrical engineering at KAIST, Daejeon, South Korea. His research interests include deep learning, multimodal learning, causal inference, object detection, and adversarial robustness.



SANGYUN CHUNG received the B.S. degree in computer science from Hanyang University, Seoul, South Korea in 2023. He is currently pursuing the M.S. in electrical engineering at KAIST, Daejeon, South Korea. His research interests include deep learning, multimodal learning, object detection, large language models, and adversarial robustness.



DAMIN YEOM received the B.S. degree in electronic and electrical engineering from Ewha Womans University, Seoul, South Korea in 2023. She is currently pursuing the M.S. in electrical engineering at KAIST, Daejeon, South Korea. Her research interests include deep learning, object detection, multimodal learning.



YOUNGJOON YU received the B.S. degree in electrical engineering from Korea Advanced Institute of Science and Technology (KAIST), Daejeon, South Korea in 2013, and the M.S. degree in the management engineering from KAIST in 2017. He is currently pursuing the Ph.D. in electrical engineering at KAIST, Daejeon, South Korea. His research interests include deep learning, multi-sensor learning, and adversarial robustness.



HAK GU KIM received the B.S. and M.S. degrees from Inha University, Incheon, South Korea, in 2012 and 2014, respectively, and the Ph.D. degree from the Korea Advanced Institute of Science and Technology (KAIST), Daejeon, South Korea, in 2019. He was a Postdoctoral Researcher with École Polytechnique Fédérale de Lausanne (EPFL), Lausanne, Switzerland. He is currently an Assistant Professor with the Graduate School of Advanced Imaging Science, Multimedia & Films (GSAIM), Chung-Ang University, Seoul, South Korea. His research

interests include deep learning and machine learning in 2D/3D/VR image and video processing and computer vision, human visual perception, and multi-modal learning.



YONG MAN RO (Senior Member, IEEE) received his Ph.D. degree from the School of Electrical Engineering at KAIST. He conducted research at various institutions, including Columbia University, the University of California, Irvine, and the Department of Electrical Engineering and Computer Sciences at the University of California, Berkeley. He also served as a visiting professor at The Edward S. Rogers Sr. Department of Electrical and Computer Engineering at the University of Toronto. He is currently ICT endowed chair professor at the School of Electrical

Engineering at KAIST. He is also the director of the Center for Applied Research in Artificial Intelligence (CARAI), the Image Video System Lab, and the Integrated Vision and Language Lab at KAIST. Throughout his career, he has conducted research on a wide range of image and video system topics. His research interests include image processing, computer vision, multimodal deep learning, integrating vision, speech, and language for AI, multimodal object and motion detection/recognition, inclusive human multimodal conversation, and analysis for interpretability and robustness of deep learning models. He received the young investigator finalist award from ISMRM in 1992 and the Scientist of the Year Award (South Korea) in 2003. He has served as a TPC member for numerous international conferences, including roles as program chair and organizer of special sessions. He was an Associate Editor for IEEE Signal Processing Letters and currently serves as an Associate Editor for IEEE Transactions on Circuits and Systems for Video Technology.